THE ASTROPHYSICAL JOURNAL, 399:533–550, 1992 November 10

INTERSTELLAR H_3O^+ AND ITS RELATION TO THE O_2 AND H_2O ABUNDANCES

T. G. PHILLIPS,[1] EWINE F. VAN DISHOECK,[2] AND JOCELYN KEENE[1]
Received 1992 March 4; accepted 1992 May 19

ABSTRACT

We present an interstellar medium study of the three reasonably accessible low-lying submillimeter lines of the H_3O^+ molecular ion at 396, 364, and 307 GHz. Emission at the frequencies of the latter two lines has previously been reported, but only from the spectroscopically confused regions Orion/KL and SgrB2. This work reports the first study of the 396 GHz line and, possibly more significantly, the detection of H_3O^+ lines in less confused regions. In particular, there is a clear detection of H_3O^+ in the W3 IRS 5 cloud where, in the case of the 396 GHz line at least, no other spectral features are visible in the observing band.

An analysis of the H_3O^+ line ratios shows that under high-density ($n_{H_2} \approx 10^6$–10^7 cm^{-3}), high-temperature conditions ($T_{kin} \gtrsim 50$ K), the 396 GHz line is about a factor of 2 stronger than the 364 GHz line, with the 307 GHz line much weaker, in agreement with the observations on sources such as W3 IRS 5, Orion/KL, and G34.3+0.15. However, for lower densities, the excitation of the 364 GHz line can be very sensitive to dust radiation pumping and it is shown that this seems to be the case in Sgr B2, resulting in the 364 GHz line being a factor of 2–3 stronger than the 396 GHz line. Under almost all conditions the 307 GHz line will be weak, the exception being for densities $n_{H_2} \gtrsim 10^7$ cm^{-3}.

H_3O^+ is an important molecular ion, intimately involved in the chemistry of oxygen and water. The fractional interstellar abundance, $x(H_3O^+)$, is shown to be typically in the range from 1×10^{-10} to 3×10^{-9}, in agreement with, or slightly below the theoretical values of (1–4) $\times 10^{-9}$. From a simple chemical model we show that if H_3O^+ is the main precursor of O_2 and H_2O, $x(H_2O) \approx 10^3 x(H_3O^+)$ and $x(O_2) \approx 10^4 x(H_3O^+)$, so providing order-of-magnitude predictions of the H_2O and O_2 abundances for the clouds observed in H_3O^+. The predicted $x(O_2) \approx 10^{-6}$–10^{-5} are close to the measured upper limits for O_2. The estimated water abundances, $x(H_2O) \approx 10^{-7}$–10^{-6}, are somewhat lower than those derived from other observations and suggest that additional processes may play a role in the water production. A possible mechanism is grain surface formation of H_2O followed by release back into the gas phase when the grains are heated to sufficiently high temperatures by radiation from newly-formed stars.

Subject headings: ISM: molecules — line: identification — molecular processes — radio lines: molecular: interstellar

1. INTRODUCTION

The molecular ion H_3O^+, or hydronium, plays a very important role in the ion-molecule reaction scheme expected to dominate the chemistry of the dense interstellar medium. Ions such as H_3^+, HCO^+, $HOCO^+$, and H_3O^+ are the protonated versions of the stable species H_2, CO, CO_2, and H_2O and their presence in the interstellar medium helps to verify the scheme (Herbst et al. 1977). H_3O^+ is the key ion for the oxygen chemistry (Herbst & Klemperer 1973; Dalgarno & Black 1976): dissociative recombination of the ion leads to OH and H_2O, and OH can subsequently rapidly react with O to form O_2. Outside of CO, chemical models predict O_2 and H_2O to be the dominant oxygen-bearing molecules in interstellar clouds. However, neither of them can easily be observed in the bulk of the interstellar medium because of blockage from the Earth's atmosphere. Observations of highly excited maser transitions of H_2O at 22 GHz (Cheung et al. 1969) and higher frequencies (Menten, Melnick, & Phillips 1990a; Menten et al. 1990b; Cernicharo et al. 1990) are available, but do not provide accurate information on column densities. Information about lower lying rotational transitions of H_2O (Waters et al. 1980; Phillips, Kwan, & Huggins 1980) and $H_2^{18}O$ (Jacq et al. 1988, 1990; Phillips et al. 1978; Wannier et al. 1991) is restricted to the cores of a few giant molecular clouds (GMCs), and, in the case of $H_2^{18}O$, is badly confused by strong lines of other molecules. Observations of near-infrared vibration-rotation absorption lines arising in low-lying H_2O levels could potentially result in accurate abundances, but are plagued by interference with atmospheric lines (Knacke & Larson 1991). HDO provides another probe of water (Turner et al. 1975; Jacq et al. 1990; Schulz et al. 1991), but again is limited to a few sources and the analysis is complicated by uncertainties in the deuteration process. Searches for molecular oxygen in interstellar clouds have focused on lines of the $^{16}O^{18}O$ isotopic variety (Black & Smith 1984), but have met negative results so far (Liszt & Vanden Bout 1985; Goldsmith et al. 1985; Combes et al. 1991; Bergman, Hjalmarson, & Booth 1992; Keene et al. 1992). Identification of the precursor H_3O^+ and a determination of its distribution in the interstellar medium is therefore very useful.

H_3O^+ is a molecular ion with its fundamental transitions lying in the submillimeter band. It is isoelectronic with ammonia (NH_3) and has the same physical structure. NH_3 has the well-known radio inversion splitting to the rotational levels and H_3O^+ might have been expected to have a similar spectrum, but with a smaller inversion splitting rather like the other similar molecules phosphine (PH_3) or arsine (AsH_3). However, Liu & Oka (1985) found that the inversion splitting was in fact very large (~ 55 cm^{-1}) and were able to predict the frequencies for the lowest lying rotation-inversion transitions. Laboratory measurements of these ground transitions were

[1] Division of Physics, Mathematics, and Astronomy, Downs Laboratory of Physics, California Institute of Technology 320-47, Pasadena, CA 91125.
[2] Leiden Observatory, P.O. Box 9513, 2300 RA Leiden, the Netherlands.

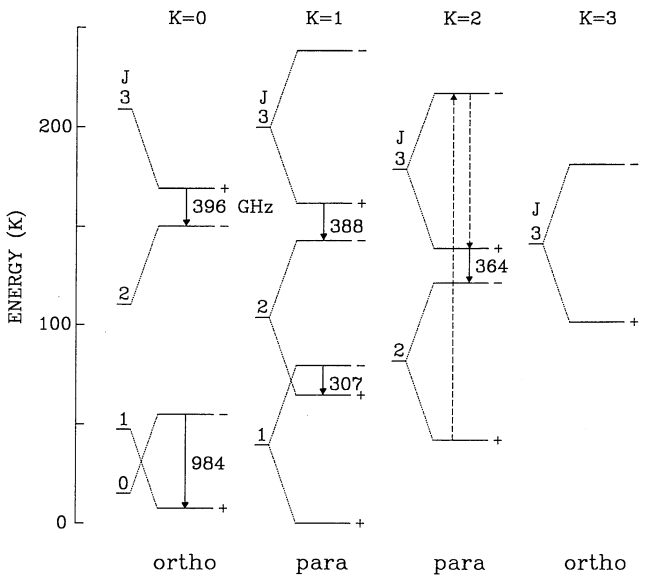

FIG. 1.—Energy level diagram of H_3O^+, illustrating the submillimeter transitions (*full lines*) and the possible radiative pumping of the 364 GHz line (*dashed lines*).

made by Plummer, Herbst, & De Lucia (1985), Bogey et al. (1985) and Verhoeve et al. (1988, 1989). An energy level diagram for the lowest four J levels is shown in Figure 1. Like NH_3, H_3O^+ has both ortho- and para-modifications, with $K = 0$ and $3n$ ortho and $K = 3n + 1$ and $3n + 2$ para. There are four reasonably accessible low-lying transitions, just in the submillimeter, at about 307, 364, 388, and 396 GHz, of which the first three belong to para-H_3O^+ and the last one to ortho-H_3O^+.

Possible detections of the 307 GHz line have been presented by Wootten et al. (1986) and Hollis et al. (1986) in the Orion OMC-1 and Sgr B2 regions. Identification of less abundant species in these two regions is always difficult due to the huge complexity of relatively broad line features: the amazing profusion of lines in the 200–270 GHz band demonstrated by Blake et al. (1987) is, if anything, more pronounced in the submillimeter band (Goesbeck, Blake, & Phillips 1992). Nevertheless it is a first step in the establishment of the presence of a new molecule or molecular ion. As will be discussed in this paper (see also Wootten et al. 1990), the 307 GHz line is probably the weakest of the available H_3O^+ lines. However, recently Wootten et al. (1991) have used the Caltech Submillimeter Observatory (CSO) to search for the 364 GHz line, and found much more convincing features in OMC-1 and Sgr B2. Of the two remaining lines, only the 396 GHz one is in a reasonably transparent region of the atmosphere and has been searched for by us, again using the CSO. This proved to be a very successful search and a feature is clearly present in OMC-1 and Sgr B2, but more importantly in several other regions such as W3, G34.3+0.15, and possibly W51. For OMC-1 the spatial distribution was determined and compared with that of other lines in the spectrum. In the particular case of W3 IRS 5 there is no line confusion at all and the H_3O^+ line was unambiguously detected. Encouraged by this result, we widened the Wootten et al. study of the 364 GHz line to the same set of regions, again with good success. For completeness the 307 GHz line was reobserved in OMC-1, Sgr B2, and in other regions, but as mentioned this line is expected to be quite weak.

We have developed an excitation calculation for H_3O^+ with certain simplifying approximations and present this, together with a discussion of the abundance of H_3O^+ and the implications for the chemistry. The analysis provides estimates for the O_2 and H_2O abundances and further emphasizes the need for more sensitive O_2 searches.

2. OBSERVATIONS

The observations were carried out at the CSO during 1990 November and 1991 February, March, and September. The receiver used was the lead alloy SIS junction system constructed by Ellison et al. (1989) with a high-frequency local oscillator borrowed from a laboratory program. The receiver double sideband noise temperature was about 350 K at 396 GHz and the telescope main beam efficiency was measured to be 55% using Mars as a calibration source. At 307 GHz the main beam efficiency was 60%. Line temperatures throughout this paper are given in terms of the chopper calibrated T_A^*-values and should be corrected by the quoted efficiency factors to derive main beam antenna temperatures. Two backend spectrometers were used in parallel, a 500 MHz broadband acousto-optical spectrometer (AOS) with an effective resolution of 1 MHz, and a 50 MHz narrow AOS with a resolution of about 100 kHz. The CSO beam size decreases from about 24″ at 307 GHz to approximately 18″ at 396 GHz. At 307 and 364 GHz, the H_3O^+ line was observed in the upper sideband, whereas at 396 GHz, the line was centered in the lower sideband. The sidebands are separated by 2.8 GHz.

The objects observed by us in the various lines are listed in Table 1. Primarily this investigation is of the 396 GHz line, but in the significant cases of W3, Orion, G34.3 + 0.15, and Sgr B2 observations were carried out at 364 GHz as well. For line search purposes, the strongest sources are Orion OMC-1 and Sgr B2 and since the work of Wootten et al. (1986, 1991) and Hollis et al. (1986) concentrated on these two objects it was natural for us to initiate our search for the 396 GHz line there also. However, as is well known, the high degree of line confusion in these objects reduces the confidence level of line identification, so other GMCs were included in the search, together with some low-mass star-formation regions and oxygen-rich circumstellar envelopes.

The results are summarized in Table 1. The most impressive detection of the H_3O^+ $J_K = 3_0^+ - 2_0^-$ line at 396 GHz is in W3 IRS 5. Here the spectrum is uncluttered by the high-excitation lines found in OMC-1 and Sgr B2. We also clearly detected the $3_2^+ - 2_2^-$ 364 GHz line in W3 IRS 5. By contrast no detections were made in W3 IRS 4, but a possible detection of the 396 GHz line is present in W3(OH). Lines at the correct frequency are clearly visible at 396 and 364 GHz for OMC-1 and Sgr B2. The 396 and 364 GHz lines are present in G34.3+0.15, and in W51 Main the 396 GHz line is possibly seen. Nothing was found in the ρ Oph sources and for the oxygen stars only VY CMa shows a hint of a line at 396 GHz. For the $1_1^- - 2_1^+$ line at 307 GHz, reasonably secure detections were made in OMC-1, G34.3 + 0.15, and W51, but no convincing features were found in W3 IRS 5 and Sgr B2.

In the following, we deal with the individual sources in the order given in Table 1. The question of line identification for all the other features in the spectra is somewhat vexing because, on average, for new submillimeter bands only about one-half of the lines appear in the current catalogs. However, for several of our sources the only visible features, apart from H_3O^+ are CH_3OH, DCN, and OCS. In OMC-1 and Sgr B2 the situation

1992ApJ...399..533P

TABLE 1

SUMMARY OF H_3O^+ OBSERVATIONS

SOURCE	α(1950)	δ(1950)	3_0^+–2_0^- 396 GHz				3_2^+–2_2^- 364 GHz				1_1^-–2_1^+ 307 GHz			
			V_{LSR} (km s^{-1})	T_A^* (K)	ΔV (km s^{-1})	$\int T_A^* dV$ (K km s^{-1})	V_{LSR} (km s^{-1})	T_A^* (K)	ΔV (km s^{-1})	$\int T_A^* dV$ (K km s^{-1})	V_{LSR} (km s^{-1})	T_A^* (K)	ΔV (km s^{-1})	$\int T_A^* dV$ (K km s^{-1})
W3 IRS 5	02^{h}21^{m}53^s.3	61°52′21″.4	−38.5	0.36	5.8 ± 0.7	2.2	−39.1	0.12	5.8 ± 0.6	0.74	...	≤0.05	...	...
W3 IRS 4	02 21 43.5	61 52 49	...	≤0.1	...	...	...	...	...	...	...	...	...	...
W3 (OH)	02 23 17.3	61 38 58	−45.0	0.20:	5.3 ± 1.0	1.1:	...	≤0.06	...	...	...	...	...	...
Orion/KL	05 32 46.8	−05 24 25	9.6	1.8	13 ± 2	25.7	8.7	0.5	9.3 ± 0.5	4.8	7.5	0.6	...	...
Orion FIR 4 30″N	05 32 45.9	−05 25 36	...	≤0.1	...	...	...	≤0.06	...	...	...	...	...	...
N2024 FIR 5 15″S	05 39 12.8	−01 57 19	...	≤0.09	...	...	...	≤0.11	...	...	...	≤0.04	...	...
ρ Oph A	16 23 25	−24 15 49	...	≤0.13	...	...	...	...	...	...	...	...	...	...
ρ Oph A SO_2	16 23 20	−24 15 49	...	≤0.12	...	...	...	...	...	...	...	...	...	...
ρ Oph B2	16 24 26.3	−24 19 49	...	...	...	...	...	...	...	...	...	...	...	...
IRAS 16293	16 29 20.8	−24 22 13	...	≤0.08	...	...	...	...	...	...	...	≤0.06	...	...
Sgr B2 (OH)	17 44 11.0	−28 22 30	64.3	0.24	15.4 ± 2	3.9	62.2	0.68	16.5 ± 0.5	11.9	...	≤0.15	...	...
Sgr B2 2′ N	17 44 09.5	−28 20 20	...	≤0.1	...	...	68.3	0.27	16.5 ± 1.5	4.7	...	...	...	...
G 34.3+0.15	18 50 46.4	01 11 14	58.0	0.23	3.6 ± 0.7	0.88	59	0.15:	4 ± 2	0.7:	58	0.2	...	...
W51 M	19 21 26.4	14 24 40.8	57.1	0.1:	6.2 ± 1.0	0.8:	...	...	...	...	56	0.25	...	...
VY CMa	07 20 54.6	−25 40 12	19	≤0.1	14:	...	...	≤0.04	...	...	...	≤0.05	...	...
OH 231.8	07 39 58.9	−14 35 43	...	≤0.1	...	...	...	≤0.05	...	...	...	...	...	...
IRC +10216	09 45 14.8	13 30 40	...	...	...	...	...	≤0.05	...	...	...	...	...	...
R Crt	10 58 06	−18 03 22	...	...	...	...	...	...	...	...	...	...	...	...
V Hya	10 49 11.3	−20 59 05	...	≤0.05	...	...	...	...	...	...	...	≤0.08	...	...
W Hya	13 46 12.1	−28 07 09	...	≤0.06	...	...	...	...	...	...	...	...	...	...

NOTES.—Upper limits are for 2 σ in a 1 MHz channel. A colon indicates an uncertain value.

is quite complex and a brief discussion of other line identifications is reserved for the Appendix.

2.1. *The W3 Region*

The W3 region is at a distance of about 2.4 kpc (Georgelin & Georgelin 1976), and contains several H II region radio sources with strong maser emission and an associated cluster of infrared sources (Wynn-Williams, Becklin, & Neugebauer 1972). Millimeter continuum observations show that the core of the W3 cloud has two main condensations of roughly equal mass, one associated with IRS 5 and the other located approximately 10″–20″ south of IRS 4 (Jaffe et al. 1983; Richardson et al. 1989). The compact infrared source W3(OH) is located about 16′ SE from the core containing IRS 5 and IRS 4. The three sources have very comparable luminosities: about $2 \times 10^5\ L_\odot$ for IRS 5 and 10^5 for both IRS 4 and W3(OH) (Werner et al. 1980; Thronson & Harper 1979).

In the earlier work on the 307 GHz line, Wootten et al. (1986) inspected the IRS 4 region without success. In searching for the 396 GHz line, we also chose IRS 4 initially, but after no clear feature was found switched to the more luminous and possibly less evolved region, IRS 5. Quickly, it was clear the line was much stronger there, $T_A^* \approx 0.4$ K, as opposed to at most 0.1 K in W3 IRS 4. Furthermore, the line confusion typical of GMC spectra was singularly lacking. The upper panel in Figure 2 shows the full 500 MHz spectrum for W3 IRS 5 with the H_3O^+ feature at the expected frequency of 396.2724 GHz. The 396 GHz line was also searched for toward W3(OH), but the feature there is marginal at best (see the summary of observations in Fig. 11, § 3). In the W3(OH) spectrum, the only other features are the 5_0–4_1 E CH_3OH line at 398.946 GHz in the image sideband and a weak unidentified line at 396.358 GHz. Toward W3 IRS 4, the CH_3OH line is seen as well, but the H_3O^+ value is given as an upper limit in Table 1.

Figure 2 includes the spectrum for the H_3O^+ line at 364.7974 GHz toward W3 IRS 5. The H_3O^+ line is clearly seen again, with a strength about $\frac{1}{3}$ of that of the 396 GHz line. Other lines in this spectrum are DCN 5–4 at 362.046 GHz and 8_1–7_2 E of CH_3OH at 361.852 GHz, both in the image sideband, and the OCS 30–29 line at 364.749 GHz in the signal sideband. Unfortunately, the DCN 5–4 and OCS 30–29 lines accidentally coincide in the spectra. In W3 (OH), the H_3O^+ 364 GHz feature is marginal or not detected (see the summary of observations in Fig. 12, § 3). Finally the 307 GHz line in W3 IRS 5 is not present at the 0.05 K level, as the bottom panel of Figure 2 illustrates. Although a feature occurs close to the frequency of the H_3O^+ 307.192 GHz line, it is shifted by about 5 km s^{-1} from the expected velocity.

The 396 and 364 GHz lines in W3 IRS 5 are displayed on an expanded scale in Figure 3. It is evident that the two lines occur at the same velocity of -39 km s^{-1} and that within the errors they have the same width of about 6 km s^{-1}. We believe that this constitutes the clearest evidence to date for the presence of H_3O^+ in the interstellar medium.

2.2. *Orion Region*

Altogether three positions were searched in the Orion region. Most effort was spent on the chemically rich Orion/KL, or IRc2 region of OMC-1, where a small map was made. Also observed were positions 30″ N of Orion FIR 4 and 15″ S of NGC 2024 FIR 5 (Mezger et al. 1988, 1990). These offsets were chosen to correspond to peaks in $C^{18}O$ maps, and are the same positions where searches for O_2 have been made (Keene et al. 1992). The only detection of an H_3O^+ feature was on Orion/KL. Figure 4 shows the full spectra at 396, 364, and 307 GHz for Orion/KL (see Figs. 11 and 12, § 3, for Orion FIR 4 and NGC 2024 FIR 5). At 396 GHz the H_3O^+ feature stands out clearly at $T_A^* \approx 2$ K, but is probably a composite of more than one line shape feature and could be contaminated by other molecules. Local oscillator shifts confirmed that the line indeed belonged to the signal sideband. The CH_3OH 5_0–4_1 E line and U 396.358 are also strong. As usual for an Orion/KL spectrum in the submillimeter, there is a host of unidentified weak features as well. Virtually all of the structure in the spectrum is due to molecular emission rather than noise. Nevertheless, the detection of a strong line at the correct frequency strengthens the identification of H_3O^+ in this source. The 364 GHz spectrum also has a clear H_3O^+ feature ($T_A^* \approx 0.5$ K)

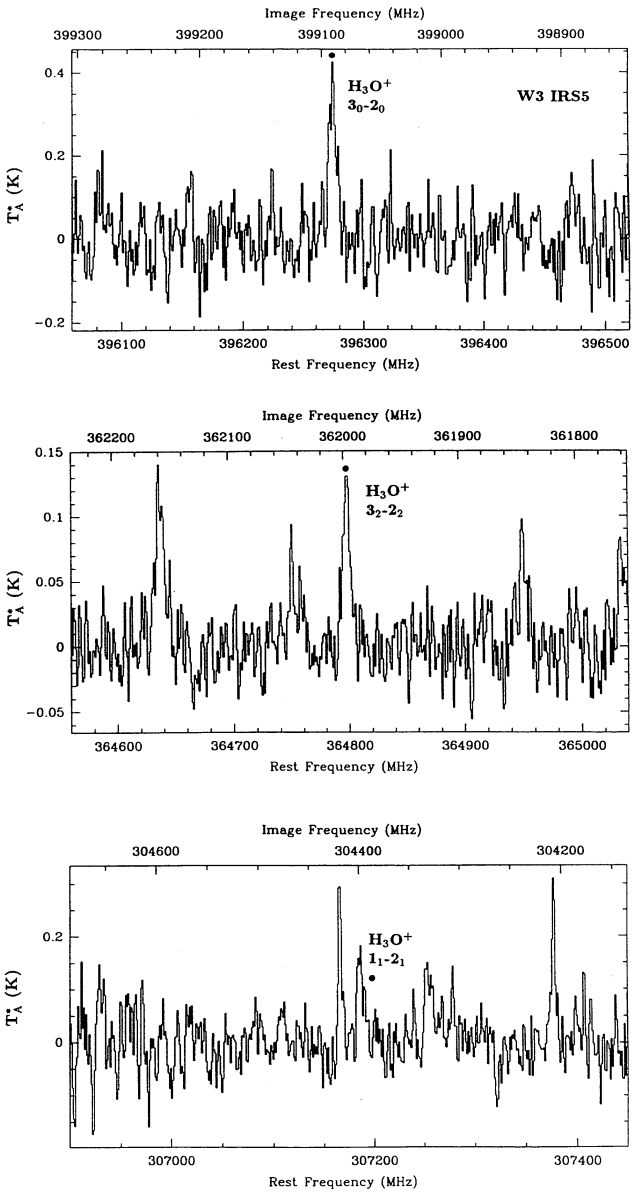

FIG. 2.—Full 500 MHz bandwidth spectra at 396 GHz (*top*), 364 GHz (*middle*) and 307 GHz (*bottom*) toward W3 IRS 5 ($V_{LSR} = -39$ km s^{-1}). The positions of the H_3O^+ lines are indicated. See Table 3 for identification of other weak features.

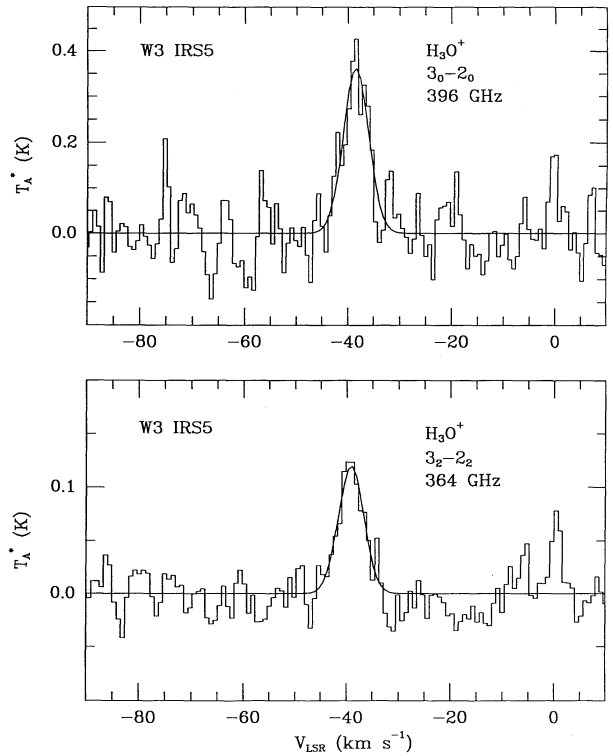

FIG. 3.—Detailed spectra of the 396 and 364 GHz H_3O^+ lines toward W3 IRS 5.

fortuitously in a gap between stronger lines. This spectrum was observed previously by Wootten et al. (1991) at the CSO and our spectrum is essentially identical with theirs. The 307 GHz spectrum is similar to the earlier ones of Wootten et al. (1986) and Hollis et al. (1986) and shows a $T_A^* \approx 0.6$ K line at the H_3O^+ frequency. The other features in the Orion spectra, including torsionally excited methanol (Anderson, Herbst, & De Lucia 1992), will be discussed briefly in the Appendix.

The 396, 364, and 307 GHz H_3O^+ features are compared in detail in Figure 5. Both the 396 and 364 GHz features appear to be composites of broad and narrow lines and each is centered roughly at 9 km s^{-1}. The ratio of peak antenna temperatures T_A^* [396/364] is nominally about 3.6 as compared to about 3 in the case of W3 IRS 5. However, the ratio of integrated antenna temperatures $\int T_A^* dV$ [396/364] in Orion is much larger than in W3 IRS 5, which is probably due to a very poorly defined baseline in the 364 GHz spectrum. It is also possible that one if not both of the Orion lines is blended with some other species. The 307 GHz line does not appear to have a broad component, although its width is difficult to determine due to blending; it is apparently centered at about 8 km s^{-1}.

In an attempt to gain additional information we made a small (6 × 5 pixel) map of the region at 396 GHz at 10″ spacing. The distribution of the strong 396 GHz H_3O^+ feature is thus compared with the 398.946 GHz CH_3OH and 396.358 GHz U line distributions. These maps are shown in Figure 6. Due to uncertainties in the absolute pointing of the telescope at the time of observations (probably up to 8″), the CH_3OH map has been taken to define the pointing, since it is known that CH_3OH is centered on the compact ridge source at about $\alpha = 05^h32^m46^s.8$; $\delta = -05°24'33''$ (1950) (e.g., Wilson et al. 1989; Mangum et al. 1990). The U396.358 line is apparently also centered on the compact ridge, suggesting that it is due to a species which has similar chemical characteristics to CH_3OH. With this registration, the H_3O^+ map is centered essentially on the position of the hot core at $\alpha = 05^h32^m47^s.0$; $\delta = -05°24'26''$ (1950); it is clearly offset by about 10″ from CH_3OH. However, on attempting to break the H_3O^+ emission into a broad and narrow component and to plot them separately, the situation is less neat. While the broad component is

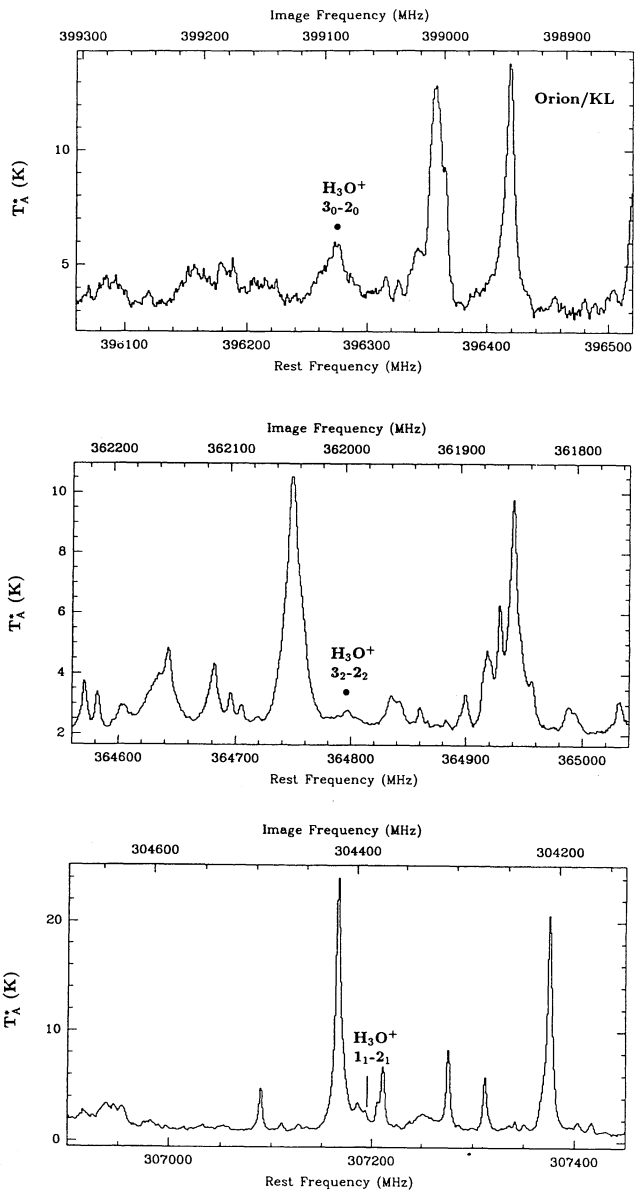

FIG. 4.—Full 500 GHz bandwidth spectra at 396 GHz (*top*), 364 GHz (*middle*) and 307 GHz (*bottom*) toward Orion/KL ($V_{LSR} = 9$ km s^{-1}). The positions of the H_3O^+ lines are indicated. In the 396 GHz spectrum, the strong feature at 398.95 GHz is due to CH_3OH 5_0–4_1 (E). The strong line at 396.36 GHz is unidentified. In the 364 GHz spectrum, the strong line at 361.85 GHz is due to CH_3OH 8_1–7_2 (E) and that at 364.75/362.05 GHz to OCS 30–29 blended with DCN 5–4. Several weak features in the spectrum can be ascribed to torsionally excited CH_3OH, but most of the lines are unidentified. In the 307 GHz spectrum, the line at 304.21 GHz is due to CH_3OH 2_1–2_0 (A), at 304.31 GHz to H_2CS 9_{19}–8_{18} and at 307.17 GHz to CH_3OH 4_1–4_0 (A). See also Table 3.

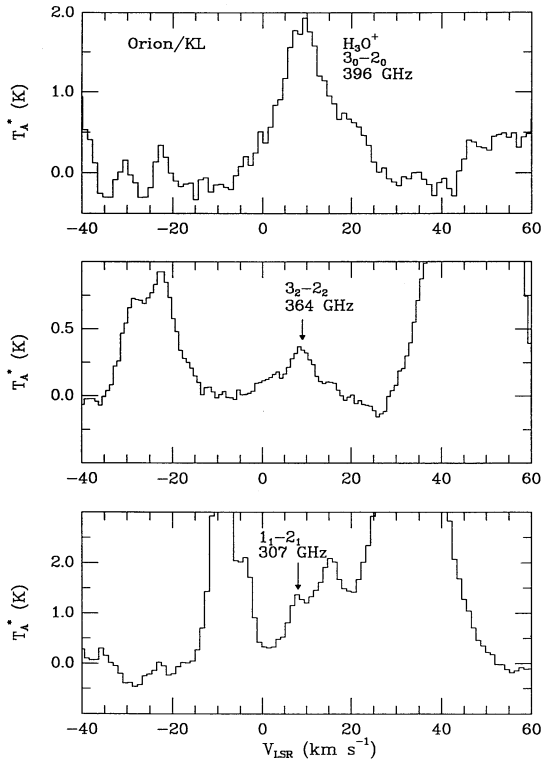

FIG. 5.—Detailed spectra of the H_3O^+ lines toward Orion/KL (linear baseline removed).

still consistent with the hot core, but distributed also to cover IRc2, the narrow component peaks more to the south at a position about 10″–20″ to the east of the compact ridge seen in CH_3OH.

No doubt the broad-line H_3O^+ distribution could be a combination of hot core and plateau emissions. The central velocity of the feature at 9 km s^{-1} is in any case dominated by the narrow feature, so that the broad line (~15 km s^{-1} wide) could be a combination of a 10 km s^{-1} wide hot core and a somewhat wider plateau line. The shape of the H_3O^+ line and its distribution are actually remarkably similar to those of HDO as presented by Plambeck & Wright (1987) and Schulz et al. (1991). If both are representative of water, it indicates that water has an affinity for the hot core.

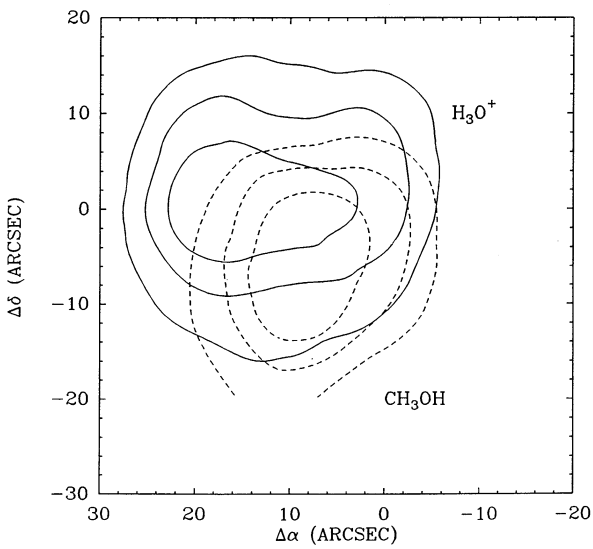

FIG. 6.—Distribution of the integrated intensity $\int T_A^* dV$ of the H_3O^+ 396 GHz line (*full contours*) and the CH_3OH 5_0–4_1 E 398.946 GHz line (*dashed contours*) toward Orion/KL. The contours are at 40%, 60%, and 80% of the maxima of 38.7 and 105.5 K km s^{-1}, respectively. The distribution of the U 396.358 GHz line is similar to that of CH_3OH. The (0, 0) position of the map is the Orion/KL position [α(1950) = 05^{h}32^{m}46^s.8, δ(1950) = −5°24′25″], but see text for uncertainties due to pointing inaccuracies.

2.3. *ρ Oph Sources*

Four positions were examined in the ρ Oph cloud (see Table 1), including the IRAS 16293−2422 low-mass star-formation region, which is a rich source of molecular lines otherwise. Apart from the CH_3OH 5_0–4_1 E transition at 399 GHz in IRAS 16293, virtually nothing was seen in the 396 GHz signal and image bands (see § 3, Fig. 11). As a result no searches were carried out in the other bands.

2.4. *The Sgr B2 Cloud*

The Sgr B2 region has been the subject of many chemical and physical studies, which have mostly focused on the warm and dense gas associated with the radio continuum sources Sgr B2(N) and (M) (Cummins, Linke, & Thaddeus 1986; Lis & Goldsmith 1989; Sutton et al. 1991; Turner 1991). Wootten et al. (1986, 1991) observed the "OH" position, which lies about 25″ south of Sgr B2(M). We observed the same position as Wootten et al., and made a clear detection of a feature at 396 GHz with $T_A^* \approx 0.24$ K. However, the feature was not seen in Sgr B2 (2′ N) where the abundance of the $HOCO^+$ ion peaks (Minh, Irvine, & Ziurys 1988), although the limit here is only $\lesssim$0.2 K (Table 1). The 5_0–4_1 methanol line was seen in both spectra. At 364 GHz, a very strong line ($T_A^* \approx 0.7$ K) is seen in Sgr B2 and quite a strong line ($T_A^* \approx 0.27$ K) in Sgr B2 (2′ N). Our spectrum at the "OH" position is essentially identical to that presented by Wootten et al. (1991). A spectrum was taken in the 307 GHz band for Sgr B2, but no convincing line was seen at the level 0.15 K at the correct velocity, in contrast with the earlier work of Wootten et al. (1986). The spectra are shown in Figure 7. As in Orion, the situation is confusing with a danger of blending, because of the large line widths.

A detailed comparison of the 396 and 364 line shapes is given in Figure 8 for Sgr B2(OH). Within the uncertainties these have the same V_{LSR} and ΔV values (63 km s^{-1} and 15 km s^{-1}, respectively). However, unlike the W3 IRS 5 case, this time the 396 GHz line is about a factor of 3 weaker than the 364 line, again with the 307 GHz line weaker yet. For Sgr B2 (2′ N), the [396/364] line ratio could well be similar, since this is allowed within the signal to noise of the 396 GHz measurement (see Table 1). It is certainly more like the Sgr B2 ratio than that for W3 IRS 5.

2.5. *G34.3+0.15 and W51*

G34.3+0.15 is a "hot core"-type region lying at a distance of about 3.7 kpc (Heaton, Little, & Bishop 1989; Henkel, Wilson, & Mauersberger 1987), whereas W51 M is a typical warm and dense giant molecular cloud core lying at about 7 kpc. The two regions have very similar spectra in the 396 GHz band (see Fig. 11, § 3) and indeed appear just as "scaled-down" versions of the Orion hot core spectrum. They show the methanol, U 396.358 and U 396.162 lines in roughly the same ratios and the H_3O^+ line weakly. In the 364 GHz band, only G34.3+0.15 was observed and the resulting spectrum shows

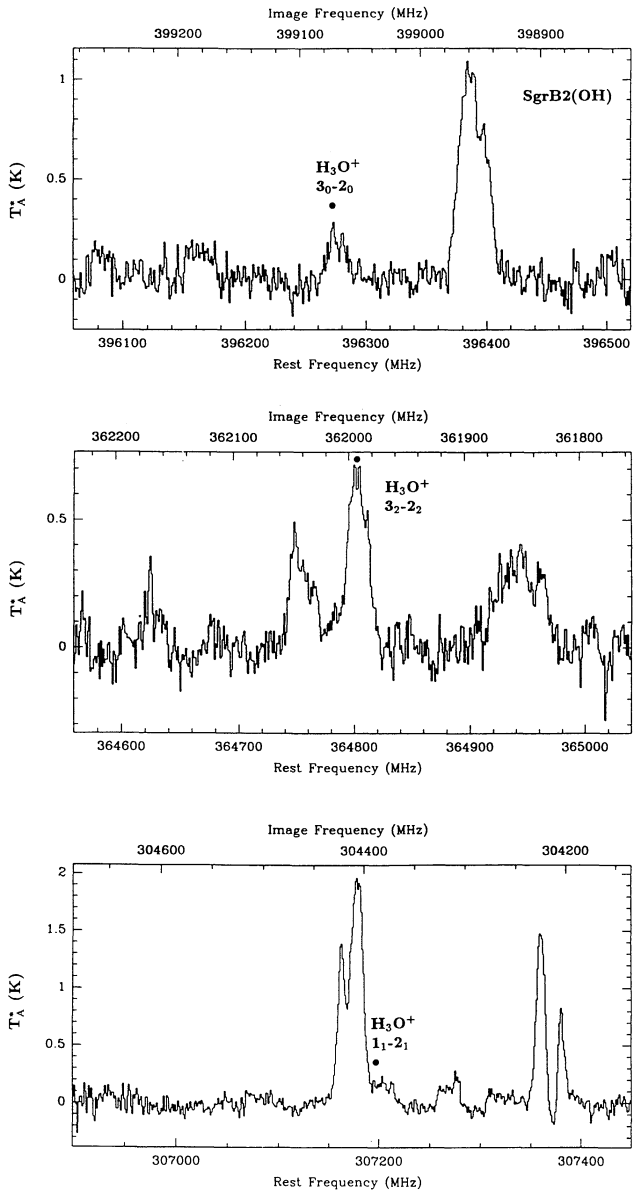

FIG. 7.—Full 500 GHz bandwidth spectra at 396 GHz (*top*), 364 GHz (*middle*), and 307 GHz (*bottom*) toward Sgr B2(OH) (V_{LSR} = 67 km s^{-1}). The positions of the H_3O^+ lines are indicated. In the 396 GHz spectrum, the strong feature at 398.95 GHz is due to CH_3OH 5_0–4_1 (E). In the 364 GHz spectrum, the line at 361.85 GHz is due to CH_3OH 8_1–7_2 (E) and that at 364.75/362.05 GHz to OCS 30–29 blended with DCN 5–4. In the 307 GHz spectrum, the line at 304.21 GHz is due to CH_3OH 2_1–2_0 (A), at 304.31 GHz to H_2CS 9_{19}–8_{18} and at 307.17 GHz to CH_3OH 4_1–4_0 (A). See also Table 3.

most of the lines found in Orion, including a weak H_3O^+ line. At 307 GHz, both W51 and G34.3+0.15 show an H_3O^+ line with $T_A^* \approx 0.2$ K. Because of blending the width of the 307 GHz line cannot be reliably determined. The three full G34.3+0.15 spectra are shown in Figure 9, and the detailed spectra in Figure 10. Again the H_3O^+ features occur at about the same V_{LSR} values (58 km s^{-1}) and have the same widths (3.5 km s^{-1}). The line ratio [396/364] in this case is about 1.7, closer to the W3 IRS 5 and Orion values than to that of Sgr B2 (Table 1).

2.6. *Oxygen Stars*

Somewhat optimistically we searched a set of mass-loss stars with oxygen rich envelopes in the 396 and 364 GHz H_3O^+ lines. In part this was for observing convenience, since no GMCs are available between the Orion and Ophiuchus regions. In addition, models by Mamon, Glassgold, & Omont (1987) predict H_3O^+ to be one of the major ions in circumstellar envelopes. Only upper limits were found, although a 2 σ double-peaked feature is present at 396 GHz in the VY CMa spectrum with the correct central velocity (see Table 1).

3. EXCITATION OF INTERSTELLAR H_3O^+ AND INFERRED ABUNDANCES

The observations presented in § 2 show that the H_3O^+ 396 GHz line has been detected in some but not all of the GMCs searched, and that the [396/364] GHz line ratio is typically 2–3, except for Sgr B2 where the ratio appears to be around 0.3. Figures 11 and 12 contain summaries of the observations. The 307 GHz line is always the weakest of the three lines. In this section, we explore the excitation of the H_3O^+ ion and the extent to which the detectability of the lines is limited by excitation. The excitation model is then used to infer H_3O^+ column densities and abundances from the observed line strengths.

3.1. *Model*

Excitation calculations for both ortho- and para-H_3O^+ were set up including all levels up to $J = 4$. The energies of the levels and the transition frequencies were generated from the spectroscopic constants given by Bogey et al. (1985) and Liu & Oka (1985). Statistical weights were obtained according to Townes & Schawlow (1955). The radiative probabilities for

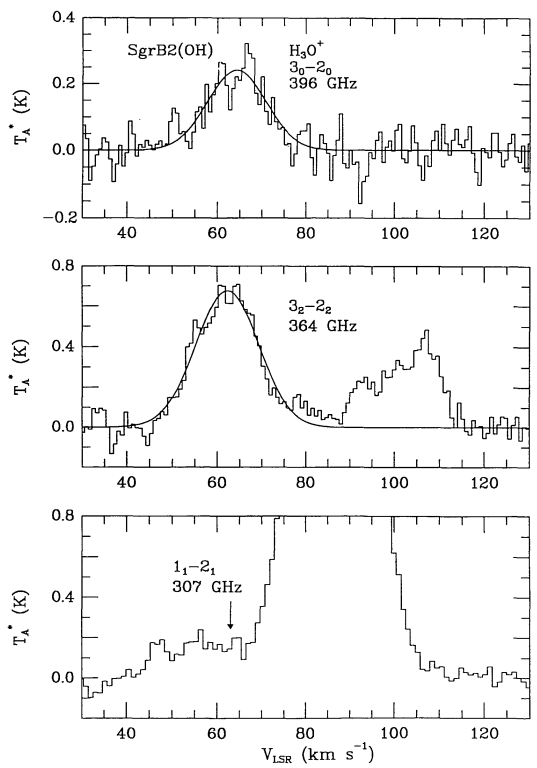

FIG. 8.—Detailed spectra of the H_3O^+ lines toward Sgr B2(OH)

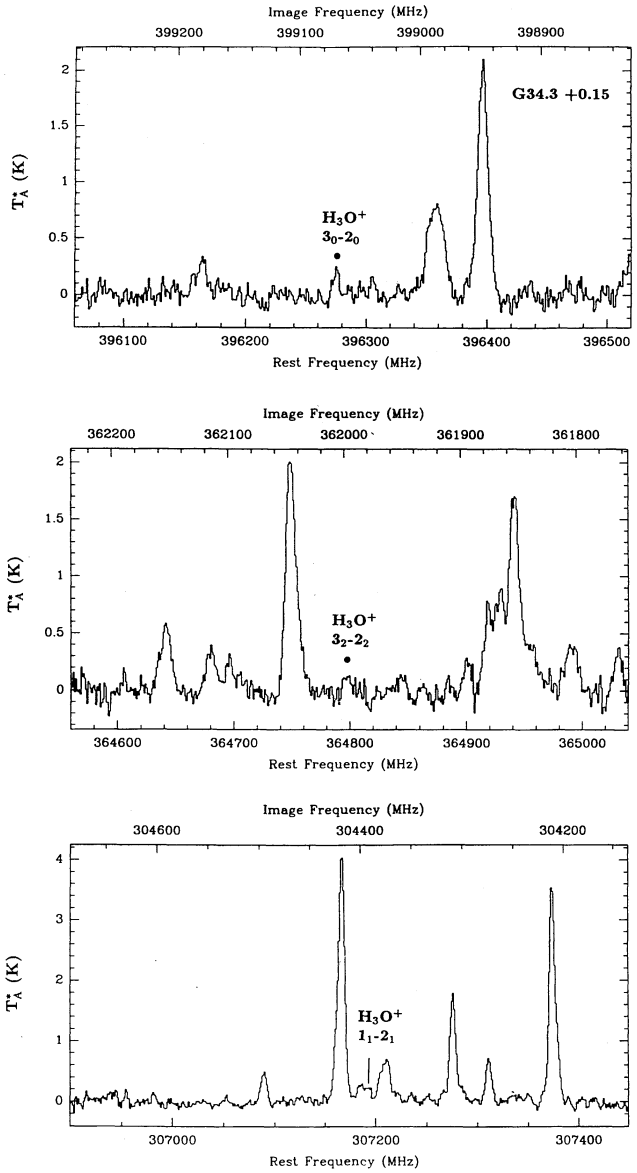

FIG. 9.—Full 500 GHz bandwidth spectra at 396 GHz (*top*), 364 GHz (*middle*) and 307 GHz (*bottom*) toward G34.3+0.15 (V_{LSR} = 59 km s^{-1}). The positions of the H_3O^+ lines are indicated. In the 396 GHz spectrum, the strong feature at 398.95 GHz is due to CH_3OH 5_0–4_1 (E). The line at 396.36 GHz is unidentified. In the 364 GHz spectrum, the strong line at 361.85 GHz is due to CH_3OH 8_1–7_2 (E) and that at 364.75/362.05 GHz to OCS 30–29 blended with DCN 5–4. Several weak features in the spectrum can be ascribed to torsionally excited CH_3OH, but most of the lines are unidentified. In the 307 GHz spectrum, the strong line at 304.21 GHz is due to CH_3OH 2_1–2_0 (A), at 304.31 GHz to H_2CS 9_{19}–8_{18} and at 307.17 GHz to CH_3OH 4_1–4_0 (A). See also Table 3.

transitions with $\Delta J = 0, \pm 1$, $\Delta K = 0$ and $+ \leftrightarrow -$ were computed using their formulae for symmetric tops with a dipole moment of 1.44 Debye, based on ab initio calculations by Botschwina, Rosmus, & Reinsch (1983). The resulting Einstein A-coefficients are large, ranging from about 5×10^{-4} s^{-1} for the transitions at 300–400 GHz to 8×10^{-1} s^{-1} for the higher frequency transitions.

The largest uncertainty in the analysis stems from the collisional rates. Since H_3O^+ is an ion, the collisional rates within one K-ladder are expected to scale with the radiative rates. Calculations for other ions such as HCO^+ (Monteiro 1984, 1985) indicate that the rate coefficients for collisional excitation of ions are usually factors of 2–6 larger than those for neutral species, because of the enhanced long-range attraction. A general collisional selection rule for symmetric tops is $\Delta K = 3n$, so that in addition to the $\Delta K = 0$ transitions, $K = 0 \leftrightarrow 3$ collisions for ortho-H_3O^+ should be fairly efficient. On the other hand, collisions which interchange $K = 1$ and $K = 2$ for para-H_3O^+ are expected to be less rapid. Finally, H-nuclei exchange reactions with H_2 are probably fast enough that the ortho/para-H_3O^+ ratio is thermalized at the present gas kinetic temperature. The ortho- and para-H_3O^+ excitations have been treated separately in this work. Test calculations of the excitation of the two species combined with an ortho/para exchange rate coefficient of 10^{-10}–10^{-9} cm^3 s^{-1} show essentially the same result.

In order to obtain an estimate of the magnitude of the rate coefficients, collisional cross sections for H_3O^+ with para-H_2 were computed within the coupled states approximation. These calculations used a model potential surface based on that for NH_3–H_2 but including the appropriate long-range terms for interaction of H_2 with an ion. Because of the large H_3O^+ inversion frequency, it has been suggested that the rigid rotor approximation may not be valid. However, test calculations which include the inversion mode in the dynamics show that the effect is very small (Offer & van Hemert 1992). The major assumption in the calculations is therefore the adopted potential surface, which may lead to factors of 3–5 uncertainties in the rates. Also, collisions with ortho-H_2 could behave differently (cf. Offer & Flower 1989; Offer & van Dishoeck 1992). Fortunately, exploratory calculations with several different sets of rate coefficients indicate that the general trends for

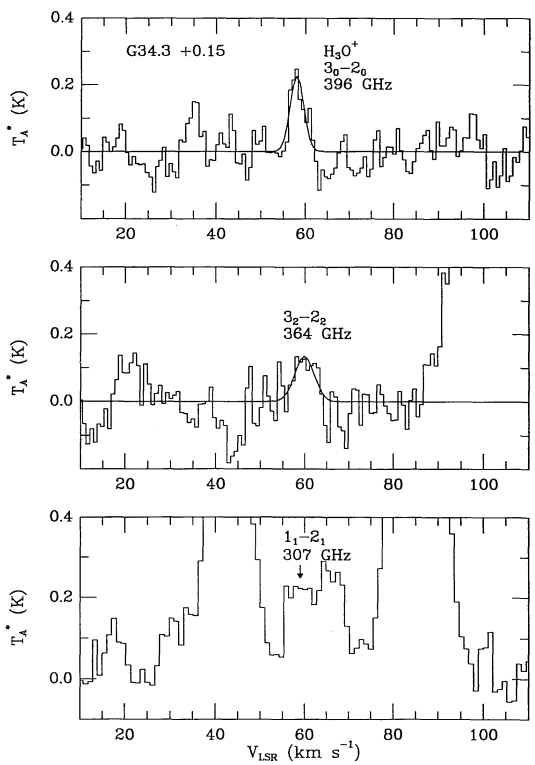

FIG. 10.—Detailed spectra of the H_3O^+ lines toward G34.3+0.15

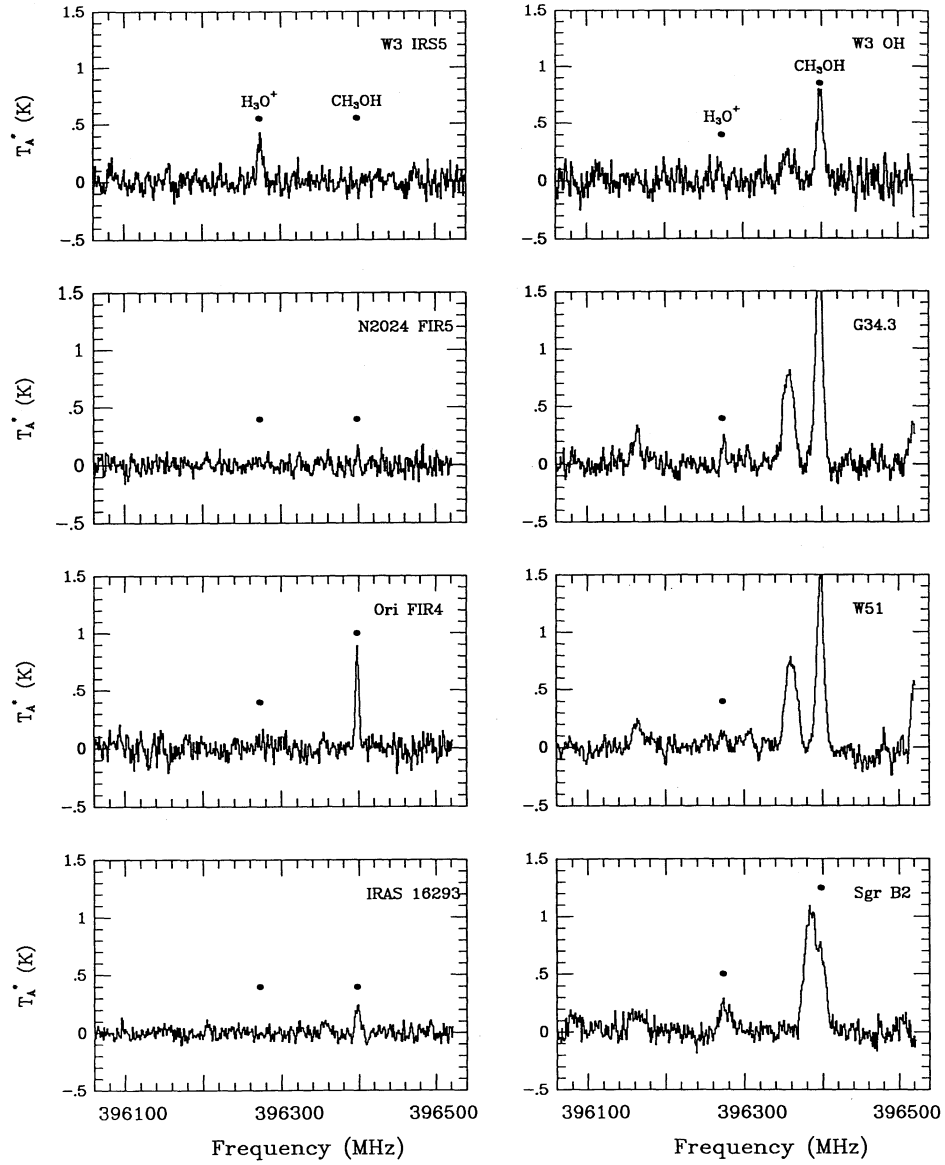

FIG. 11.—Summary and comparison of 396 GHz spectra obtained toward various sources. The positions of the H_3O^+ 3_0^+–2_0^- and CH_3OH 5_0–4_1 E lines are indicated. The strong feature at 396.36 GHz is unidentified. Note the similarity between the spectra of W51 M and G34.3+0.15, and the absence of lines in NGC 2024 FIR 5.

the transitions of interest are not particularly sensitive to the details.

The computed collisional de-excitation rate coefficients at $T = 100$ K for the 307–396 GHz transitions are of order 5×10^{-10} cm^3 s^{-1}, so that the critical densities are typically a few $\times 10^6$ cm^{-3}. Because the Einstein A-coefficient for the 364 GHz transition is a factor 2.3 smaller than that for the 396 GHz line, its critical density tends to lie somewhat lower. For the higher frequency transitions such as the 0_0–1_1 at 984 GHz, collisional processes start to dominate only at densities of order 10^8–10^{10} cm^{-3}, if the lines are optically thin.

3.2. *General Results*

Statistical equilibrium calculations have been performed for temperatures ranging from 20–200 K and densities from 10^4–10^8 cm^{-3}. Initially, stimulated absorption and emission in a background radiation field were neglected. The radiative transfer was treated with an escape probability method, in which the results scale with the ratio of the H_3O^+ column density N and the line width ΔV. Results are presented in terms of T_R, the Rayleigh-Jeans approximation to the radiation temperature. As mentioned above, ortho- and para-H_3O^+ are considered separately, and most results refer to an ortho/para ratio of unity, which is the high-temperature limit. At low temperatures, $T \lesssim 50$ K, para-H_3O^+ becomes a factor of 2 more abundant, if the ortho/para ratio is thermalized.

Several general conclusions can be drawn. First, the strengths of the 396, 388, and 364 GHz lines are comparable within a factor of 2 or 3 over the full range of conditions (assuming ortho/para = 1). In contrast, the 307 GHz line is significantly weaker (by factors of 10–100) at low densities, $n < 10^7$ cm^{-3}. This result is illustrated in Figure 13, which shows the computed antenna temperatures of the 396, 364, and 307 GHz lines as functions of density for a temperature of 100

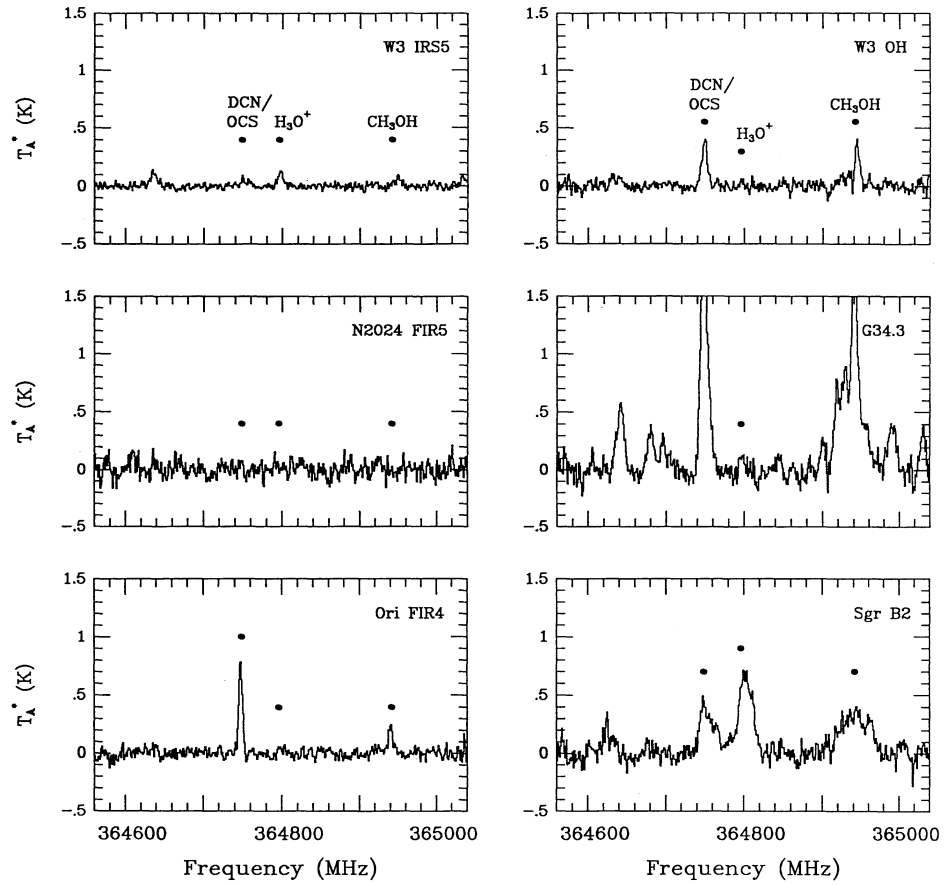

FIG. 12.—Summary and comparison of 364 GHz spectra obtained toward various sources. The positions of the H_3O^+ 3_2^+–2_2^-, CH_3OH 8_1–7_2 E, DCN 5–4 and OCS 30–29 lines are indicated.

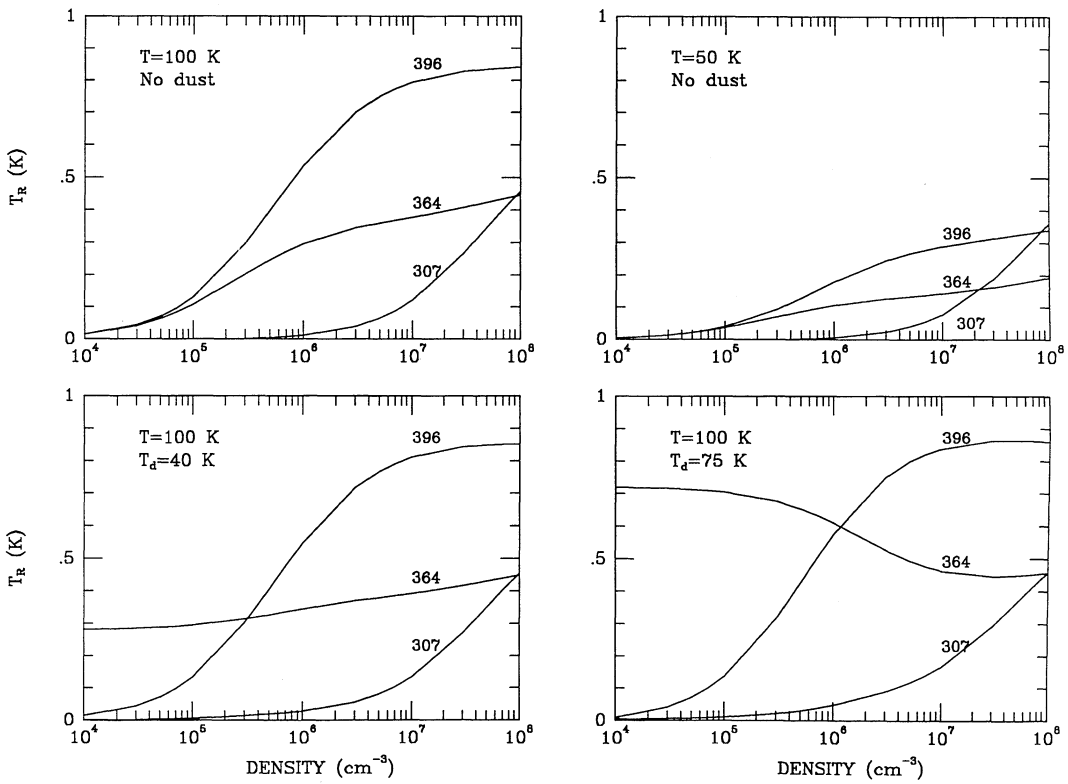

FIG. 13.—Calculated antenna temperatures T_R in K for the H_3O^+ 396, 364, and 307 GHz lines as functions of density $n(H_2)$. The four panels indicate results for various values of gas kinetic temperature and dust temperature. For the cases where dust is included we assume $E(B-V) = 60$ mag. All calculations adopt N(ortho-H_3O^+) = N(para-H_3O^+) = 5×10^{13} cm^{-2}, and $\Delta V = 10$ km s^{-1}. The results scale with $N/\Delta V$. The strength of the 388 GHz line is similar to that of the 364 GHz line in the absence of far-infrared radiation.

K. The reason for this behavior stems from the unusual energy level structure of the molecule (see Fig. 1): the upper level 1_1^- of the 307 GHz line can decay not only to the 2_1^+ level, but also to the 1_1^+ level. Because of the ν^3 factor, the A-coefficient for this latter transition is nearly an order of magnitude larger than that for the 307 GHz transition, so that the 1_1^- level is depleted very rapidly. In contrast, the upper levels 3_K^+ for the other transitions can only radiate to the 2_K^- levels. As a result, the excitation temperature for the 307 GHz transition is very low at low densities, a conclusion also reached by Wootten et al. (1990, 1991). Only at densities $n > 10^7$ cm^{-3} does the 307 GHz line become comparable in intensity to the other three lines. The low-lying 984 GHz line of ortho-H_3O^+ is usually weaker than the 396 GHz line, especially at low densities.

Second, the strengths of the 396, 388, and 364 GHz lines decrease rapidly with temperature for $T < 100$ K. As Figure 13 shows, the lines are a factor of 3 weaker at $T = 50$ K compared with $T = 100$ K. At $T = 20$ K, they are nearly two orders of magnitude weaker. Because the 307 GHz transition involves lower lying levels, this line is favored at low temperatures, $T \lesssim 50$ K.

Third, the optical depths in the 396, 388, and 364 GHz lines remain small for all reasonable H_3O^+ abundances, so that their strengths scale linearly with column density. In fact, all three lines are weakly masing in the sense that they have negative excitation temperatures. This is because the lower level of each of the transitions, level 2_K^-, radiates very rapidly to the 1_K^+ and 2_K^+ levels, resulting in rapid depletion of the lower level (see Fig. 1).

Fourth, the results for the para-H_3O^+ 364 GHz transition are significantly affected if excitation by far-infrared radiation due to dust is taken into account. This is illustrated in the lower two panels of Figure 13, which assume $T_d = 40$ and 75 K, respectively. Here the ambient dust radiation field was represented by

$$I_\nu^b = \eta B_\nu(T_d)\{1 - \exp(-\tau_d)\} \text{ ergs s}^{-1} \text{ cm}^{-2} \text{ Hz}^{-1} \text{ sr}^{-1}, \quad (1)$$

where B_ν is the Planck function at the dust temperature T_d and the dust extinction τ_d is taken from Becklin et al. (1978) between 4.8 and 50 μm and extrapolated to longer wavelengths assuming a $\lambda^{-1.5}$ dependence. A total dust column corresponding to $E(B-V) \approx 60$ mag was adopted, which is representative of the clouds observed in this work. The geometrical dilution factor η was taken to be 0.5.

For dust temperatures $T_d < 30$ K, the results appear little affected by the radiation field. However, for higher dust temperatures, the 364 GHz line is significantly enhanced with respect to the 396 GHz line at low densities, as Figure 13 shows. This is due to the fact that the upper level 3_2^+ of the 364 GHz transition can be significantly pumped by far-infrared radiation in the $3_2^- \leftarrow 2_2^+$ transition around 82 μm, followed by radiative decay of $3_2^- \rightarrow 3_2^+$ (see Fig. 1). In contrast, no such process is possible in the $K = 0$ ladder, since the $2_0^- \leftarrow 1_0^+$ transition around 100 μm only pumps the lower level of the 396 GHz line. For the 307 GHz transition, excitation through the $1_2^- \leftarrow 1_1^+$ transition at 180 μm can be efficient at lower dust temperatures, but for the 388 GHz line there is no efficient single-step process. At higher densities, $n \gtrsim 10^6$ cm^{-3}, collisional excitation starts to compete, so that the results become similar to the case without radiative excitation.

The computed [396/364] ratio is about 1.5–2 at high densities $n \gtrsim 10^6$ cm^{-3} for an ortho/para ratio of unity. Since para-H_3O^+ is more abundant at low temperatures than ortho-H_3O^+, the models actually predict [396/364] $\approx$ 1–2. The observed ratio [396/364] is generally somewhat higher, about 3. However, the computed ratio is sensitive to the details of the collisional cross sections. Since the collisional rates are uncertain by at least a factor of 3, we consider the discrepancy between the observed and predicted ratios not significant. On the other hand, the different ratio [396/364] around 0.3 found for Sgr B2 can only be explained within the current models if the H_3O^+ is in a region of lower density, $n \approx 10^5$ cm^{-3}, and if radiative excitation is significant. The predicted ratio [364/307] $\approx$ 50 under those conditions is consistent with observed value [364/307] $\gtrsim$ 10. The presence of the 307 GHz line in the spectra of Orion/KL, G34.3+0.15 and W51 M with [307/364] $\approx$ 1 requires $n \approx 10^7$–10^8 cm^{-3} in those regions.

3.3. H_3O^+ *Column Densities*

Since the line strengths depend on density, column density, temperature, and far-infrared radiation field, independent constraints on some of these parameters are necessary to infer the H_3O^+ column densities in the various clouds. In the following, we will use primarily the 396 GHz data. As explained before, this line has the big advantage that far-infrared radiation does not influence the results.

Consider first as an example the case of W3 IRS 5. Far-infrared and submillimeter continuum studies indicate dust temperatures ranging from 50–100 K (Werner et al. 1980; Gordon 1987), and on a larger scale the dust and gas temperatures are comparable in W3 (Phillips et al. 1981). The fact that the CO $7 \rightarrow 6$, $9 \rightarrow 8$, and [C I] $^3P_2 \rightarrow {}^3P_1$ lines arising from levels which lie respectively 155, 250, and 62 K above the ground state are readily detected toward W3 IRS 5 (Krügel et al. 1989; Boreiko & Betz 1991; Zmuidzinas, Betz, & Goldhaber 1986), suggests the presence of a substantial amount of warm gas with $T \gtrsim 60$ K. Note also that the CH_3OH 8_1–7_2 line, which is detected in the 364 GHz spectrum, comes from a level lying at 105 K. Finally, an analysis of H_2CO submillimeter lines arising from different K-ladders suggests $T \approx 80$–100 K (Helmich et al. 1992). Accordingly, we adopt $T = 50$–100 K in the H_3O^+ analysis, with the higher temperature the more likely value. Estimates of the density can be made from comparison of the strengths of the $C^{34}S$ 2–1, 5–4, and 7–6 lines, which suggest $n > 5 \times 10^5$ cm^{-3} (Wilson, Johnston, & Mauersberger 1991; Helmich et al. 1992). The limit on the H_3O^+ 307 GHz line indicates $n \lesssim 5 \times 10^7$ cm^{-3}. We adopt $n \approx 5 \times 10^5$–10^7 cm^{-3} in the calculations. As Figure 13 shows, the dependence of the 396 GHz antenna temperature on density is rather flat for $n \gtrsim 10^6$ cm^{-3} so that the line is primarily sensitive to column density. The observed main beam temperature, $T_{MB} \approx 0.7$ K, then corresponds to N(ortho-H_3O^+) $\approx (3$–$10) \times 10^{13}$ cm^{-2}. Assuming that the ortho/para ratio is thermalized, this results in a total H_3O^+ column density of $N_T(H_3O^+) \approx (0.6$–$3) \times 10^{14}$ cm^{-2}. The total column density of H_2 toward W3 IRS 5 can be estimated from observations of weak isotopic CO lines (Schwartz, Snell, & Schloerb 1989; Hayashi, Kobayashi, & Hasegawa 1989; Keene et al. 1992), or from submillimeter continuum measurements (Richardson et al. 1989), which suggest $N(H_2) \approx (1$–$2) \times 10^{23}$ cm^{-2} in a comparable beam. The resulting abundance of H_3O^+ is thus 3×10^{-10}–3×10^{-9}, with the lower values corresponding to the higher temperatures.

Similar determinations of the H_3O^+ column density can be made toward the other sources for which we have obtained detections, or upper limits, for the 396 GHz line. The results

TABLE 2

DERIVED INTERSTELLAR H_3O^+ COLUMN DENSITIES AND ABUNDANCES

Source	T (K)	n (cm^{-3})	$N(H_3O^+)$ (cm^{-2})	$N(H_2)$ (cm^{-2})	$x(H_3O^+)$	References
W3 IRS 5	50–100	5(5)–1(7)	(0.6–3)(14)	(1–2)(23)	3(−10)–3(−9)	1
W3 IRS 4	50–100	5(5)–1(7)	<1(14)	(1–2)(23)	<1(−9)	2
W3(OH)	50–100	5(5)–1(7)	(0.3–1)(14)	(1–2)(23)	1(−10)–1(−9)	3
Orion/KL	80–300	1(6)–1(8)	(3–7)(14)	(3–10)(23)	3(−10)–2(−9)	4
Orion FIR 4	50–100	5(5)–1(7)	<1(14)	(1–3)(23)	<1(−9)	5, 6
N2024 FIR 5	50–100	5(5)–1(7)	<1(14)	(1–3)(23)	<1(−9)	6, 7
ρ Oph A	40–80	5(5)–5(6)	<1(14)	(0.4–1)(23)	<3(−9)	6, 8, 9
ρ Oph A SO_2	40–80	5(5)–5(6)	<1(14)	(0.4–1)(23)	<3(−9)	8, 9
IRAS 16293	50–100	1(6)–1(7)	<4(13)	2(23)	<2(−10)	10
Sgr B2(OH)	50–100	5(4)–5(5)	(3–5)(14)	1(24)	3(−10)–5(−10)	11
Sgr B2 2′ N	50–100	5(4)–5(5)	(1–3)(14)	4(23)	3(−10)–1(−9)	11
G34.3+0.15	50–100	1(6)–5(7)	(0.2–1)(14)	(1–3)(23)	7(−11)–1(−9)	12, 13
W51 M	50–100	1(6)–5(7)	(0.2–1)(14)	(4–8)(23)	2(−11)–3(−10)	6, 14

REFERENCES.—(1) See text; (2) Richardson et al. 1989; (3) Wilson et al. 1991; (4) Blake et al. 1987; (5) Mezger et al. 1990; (6) Keene et al. 1992; (7) Mezger et al. 1988; (8) Wootten & Loren 1987; (9) Loren et al. 1990; (10) Mundy et al. 1990; (11) Lis et al. 1991; (12) Jacq et al. 1988, 1990; (13) Heaton et al. 1987; (14) Jaffe et al. 1984.

are summarized in Table 2, which also includes the range of physical conditions appropriate for the regions (see § 5 for a discussion). The gas temperature is obviously a critical parameter: the lower the adopted temperature, the higher the derived column density or upper limit. Many of our clouds are warm GMCs or star-forming regions for which we have assumed $T \gtrsim 50$ K. Only the ρ Ophiuchi clouds (excepting probably the IRAS 16293−2422 star-forming region) may be somewhat colder. Regarding densities, most of the clouds have $n \gtrsim 5 \times 10^5$ cm^{-3}, and therefore lie in the regime where radiative excitation is not important, consistent with the weakness of the 364 GHz line relative to the 396 GHz line. As discussed above, the detection of the 307 GHz line in Orion, G34.3+0.15 and W51 M implies $n > 10^7$ cm^{-3} in those regions, consistent with other estimates of the density in hot cores. Only in Sgr B2 does the [396/364] ratio suggest a lower density, $n \approx 10^5$ cm^{-3}. Using these physical conditions, we see from Table 2 that the inferred H_3O^+ abundances are typically a few $\times 10^{-10}$–10^{-9} for sources where the ion is detected. Unfortunately, the dynamic range of the observations is not large and the (2 σ) upper limits for other sources are of similar magnitude; the most significant limit is that toward IRAS 16293−2422, where the abundance is at most 10^{-10}, and probably even less. A significant uncertainty in the abundance determination is introduced by the poor constraints on the H_2 column densities along the line of sight. Our derived H_3O^+ column densities for Orion/KL and Sgr B2 are somewhat smaller than those found by Wootten et al. (1991) from the 364 GHz line, which results mostly from the fact that they assumed an ortho/para ratio of 3, rather than the appropriate value which tends to 1 in the high-temperature limit (see §§ 3.1 and 3.2).

4. CHEMISTRY OF H_3O^+

4.1. *Simple Model*

The H_3O^+ ion is thought to be formed in dense interstellar clouds through a simple sequence of ion-molecule reactions described in detail by Herbst & Klemperer (1973) and Herbst et al. (1977). The ion is destroyed primarily by dissociative recombination with electrons. Thus, in steady state the H_3O^+ density is given by

$$n(H_3O^+) = \frac{k_1 n(O) n(H_3^+) + k_2 n(O) n(H^+) + k_3 n(H_2O) n(H_3^+)}{k_{DR}\, n(e)}, \quad (2)$$

where formation of the ion through reactions of HCO^+ with H_2O has initially been neglected (see also § 4.2). Here k is the relevant reaction rate coefficient. The relative importance of the first and the last formation routes is determined by the ratio $n(O)/n(H_2O)$ in the clouds, which is not known observationally. Chemical models (e.g., Herbst & Leung 1989; Langer & Graedel 1989) suggest $n(O)/n(H_2O) \approx 10$–100. Since $k_3 \approx 8k_1$, the two routes may be comparable if the H_2O abundance in the cloud is sufficiently high. The relative importance of the first route versus the second route depends on the ratio $n(H_3^+)/n(H^+)$ and on the temperature, since k_2 decreases rapidly for $T < 227$ K.

The H_3^+ density in the cloud depends on the cosmic ray ionization rate ζ and can be written (Lepp, Dalgarno, & Sternberg 1987; Black et al. 1990)

$$n(H_3^+) = \frac{0.9\zeta n(H_2)}{k_4\{n(CO) + n(O) + \cdots\}}, \quad (3)$$

which for $\{n(CO) + n(O) + \cdots\}/n(H_2) \approx 10^{-4}$, $k_4 \approx 10^{-9}$ cm^3 s^{-1}, and $\zeta \approx 10^{-17}$ s^{-1} gives $n(H_3^+) \approx 10^{-4}$ cm^{-3}. The H^+ density also depends on ζ, but this ion is primarily destroyed by reactions with O, O_2, and H_2O. Typically, $n(H^+) < n(H_3^+)$, so that at low temperatures the first route dominates. If we substitute equation (3) into equation (2), neglect the second route, and assume $T \approx 70$ K, we find

$$x(H_3O^+) = \frac{n(H_3O^+)}{n(H_2)} \approx \frac{3 \times 10^{-12}}{n(e)} \left(\frac{n(H_3^+)}{10^{-4}\ cm^{-3}}\right) \times \left(\frac{x(O)}{5 \times 10^{-5}} + \frac{x(H_2O)}{7 \times 10^{-6}}\right). \quad (4)$$

This equation illustrates that the electron density $n(e)$ is a crucial parameter in the calculation of the H_3O^+ abundance. In the models, the electron density is put equal to the sum of the densities of the positive ions. If the gas-phase abundances of species such as S and Si are high ($\gtrsim$10% of solar), these "metal" ions are the most abundant ones. Otherwise, H_3^+, HCO^+, H_3O^+, and H^+ are the most abundant ions. From the observational side, the electron density in dense clouds is poorly constrained, but analysis of DCO^+ and HCO^+ measurements suggests $x(e) = n(e)/n(H_2) \lesssim 10^{-6}$, so that a low metal abundance is thought to apply. If we use the model results of $x(e) \approx 3 \times 10^{-8}$ for $n(H_2) \approx 10^5$ cm^{-3}, then

$n(e) \approx 0.003$ cm^{-3} so that $x(H_3O^+) \approx 10^{-9}$. Alternatively, if we assume typically $n(H_3^+)/n(e) \approx 0.1$, then $x(H_3O^+) \approx 3 \times 10^{-9}$ is obtained. These abundances agree well with the values $x(H_3O^+) \approx (1\text{–}4) \times 10^{-9}$ found in the much more detailed models of Herbst & Leung (1989), Langer & Graedel (1989), and Millar et al. (1991b) and are consistent with, or slightly higher than, the range of observed values (see Table 2). The detailed models also show that the H_3O^+ abundance is not strongly time-dependent.

As explained in the introduction, the abundance of H_3O^+ is directly linked to that of O_2 and H_2O. The branching ratio to form OH from the dissociative recombination of H_3O^+ has been measured by Herd, Adams, & Smith (1990) to be $f_1 \approx 0.65$. If we furthermore assume that all OH is transformed into O_2 by reactions with O, we find

$$n(O_2) = \frac{k_{DR} f_1 n(H_3O^+) n(e)}{k_5 n(\text{destructive ions})} . \quad (5)$$

The destruction of O_2 is dominated by reactions with positive ions, such as H^+, He^+, C^+, and H_3^+. However, a large fraction of the destructions results in species which eventually lead back to O_2, so that no net removal occurs. If we assume n(destructive ions)/n(ions) ≈ 0.1, $n(e) = n$(ions), and $k_5 \approx 10^{-9}$ cm^3 s^{-1}, we obtain the interesting result:

$$\frac{n(O_2)}{n(H_3O^+)} = \frac{x(O_2)}{x(H_3O^+)} \approx 10 \frac{k_{DR} f_1}{k_5} \approx 10^4 . \quad (6)$$

A lower limit can be obtained if all ions are destructive, $x(O_2)/x(H_3O^+) \approx 1000$. Thus, for $x(H_3O^+) \approx 10^{-10}$–$10^{-9}$, this would imply $x(O_2) \approx 10^{-6}$–10^{-5}, which is comparable to the most sensitive upper limits on the O_2 abundance to date (Liszt & Vanden Bout 1985; Keene et al. 1992). Sensitive searches for the $^{16}O^{18}O$ lines at positions where H_3O^+ has been detected will therefore be very valuable. We note that if the O_2 abundance is indeed significantly below 10^{-5}, O_2 comprises less than 4% of the available oxygen in the cloud, which is substantially lower than found in most gas-phase models.

The derivation of the H_2O abundance is less straightforward because the branching ratio f_2 to form water in the dissociative recombination of H_3O^+ is not known from experiments. If we take $f_2 = 0.35$ (Bates 1991) and assume that H_2O is destroyed by the same ions with a rate coefficient of 5×10^{-9} cm^{-3} s^{-1}, we find

$$\frac{x(H_2O)}{x(H_3O^+)} \approx 1000 , \quad (7)$$

within an order of magnitude uncertainty. For comparison, the detailed models of Herbst & Leung (1989), Langer & Graedel (1989), and Millar et al. (1991b) give $x(O_2)/x(H_3O^+) \approx 10^4$–$4 \times 10^4$ and $x(H_2O)/x(H_3O^+) \approx 500$–$2000$.

Equation (7) assumes that all H_2O results from the H_3O^+ chemistry cycle. In fact, the H_3O^+ abundances in clouds where the ion has been detected imply $x(H_2O) \approx 10^{-7}$–10^{-6}, which, in spite of the uncertainties in the models, seem significantly lower than the H_2O abundances of 10^{-6}–10^{-5} in these clouds derived from other observations (see § 5). In dense star-forming regions, H_2O may also be produced by surface reactions on grains during the protostellar phase with subsequent release back into the gas phase when the radiation from the newly formed star has heated the grains to sufficiently high temperatures (Brown, Charnley, & Millar 1988). If all observed H_3O^+ resulted from the H_2O with H_3^+ reaction only, gas-phase water abundances of order 10^{-5} would be required.

4.2. *Comparison of* H_3O^+ *and* HCO^+ *Chemistry*

It is instructive to compare the chemistry of H_3O^+ with that of the more widely observed HCO^+ ion, since their chemistries are linked at high densities through the reaction

$$HCO^+ + H_2O \rightarrow H_3O^+ + CO . \quad (8)$$

HCO^+ is formed mostly through the reactions of CO with H_3^+ and of C^+ with H_2O. At low densities, the ion is primarily destroyed by dissociative recombination, whereas at high densities, removal by H_2O through reaction (8) becomes effective. If we assume that most of the C^+ deep inside the clouds results from destruction of CO by He^+, and if $n(H_2O)/n(H_2) \lesssim 10^{-5}$, the reaction of CO with H_3^+ dominates the formation of HCO^+ and the computed abundance is an order of magnitude larger than that of H_3O^+, about 10^{-8}.

In order to explore the dependence of the H_3O^+ and HCO^+ abundances on the various physical parameters, the above reactions have been incorporated into a simple numerical model, which takes the CO, O, O_2, and H_2O abundances as free parameters. The model is appropriate for low metal abundances ($\lesssim$10% of solar) and takes no recombination with dust into account. Figure 14 illustrates the computed abundances of H_3O^+ and HCO^+ with respect to H_2 as functions of density for $\zeta \approx 1 \times 10^{-17}$ s^{-1} and $x(CO) = 10^{-4}$, $x(O) = 5 \times 10^{-5}$, $x(O_2) = 10^{-5}$ and $x(H_2O) = 10^{-6}$. The abundance of the H_3O^+ ion appears to depend only weakly on density. This is because the densities of the ions H^+ and H_3^+ are virtually independent of H_2 density (cf. eq. [3]), so that the electron density $n(e)$ varies only weakly with H_2 density, as long as these ions are dominant. The HCO^+ abundance shows a stronger dependence because it is removed primarily by H_2O at higher densities. Similarly, the abundance of H_3O^+ depends little on the adopted cosmic ray ionization rate, as the right panel of Figure 14 shows. Although the abundances of the principal ions increase with ζ, the electron abundance also increases, so that the enhancement is at most proportional to $\zeta^{1/2}$. Note that the same result holds for other sources of ionization, such as X-ray ionization (Krolik & Kallman 1983).

In contrast, both HCO^+ and H_3O^+ are very sensitive to the adopted H_2O abundance in the model, as the left panel of Figure 14 demonstrates. For HCO^+, reaction (8) readily becomes the dominant destruction route for $x(H_2O) > 10^{-6}$, so that the HCO^+ abundance decreases. In the case of H_3O^+, an enhancement occurs at low densities when the H_2O with H_3^+ formation route becomes equally fast to the O with H_3^+ route (cf. eq. [2]). At high densities and high H_2O abundances, reaction (8) becomes a significant formation channel of H_3O^+ at the expense of HCO^+. This effect is also found in the models of Millar, Herbst, & Charnley (1991a) for oxygen-containing molecules in the Orion compact ridge. Thus, the relative abundances of H_3O^+ and HCO^+ depend sensitively on the amount of H_2O in the gas phase at high densities, which may provide an explanation for possible variations in HCO^+/H_3O^+ abundance ratios in some clouds (see § 5).

Although the models presented in Figure 14 are greatly simplified, they have the advantage that they take the H_2O and O_2 abundances as free parameters which can be adjusted to fit the observational constraints. The main motivation for this approach is that the detailed gas-phase models usually give O_2 abundances of order (5–9) $\times 10^{-5}$, significantly higher than

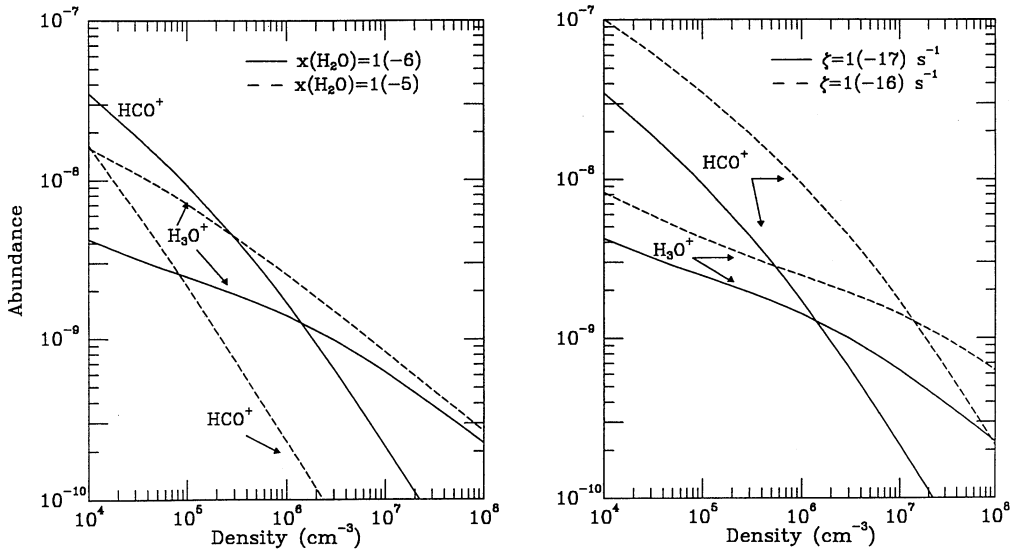

FIG. 14.—H_3O^+ and HCO^+ abundances as functions of density according to the simple chemistry described in § 4. (*Left panel*) Effect of gas-phase H_2O abundance; *full line:* $x(H_2O) = 10^{-6}$; *dashed line:* $x(H_2O) = 10^{-5}$; (*Right panel*) Effect of cosmic ray ionization rate; *full line:* $\zeta = 10^{-17}$ s^{-1}; *dashed line:* $\zeta = 10^{-16}$ s^{-1}. All models have $x(CO) = 10^{-4}$, $x(O_2) = 10^{-5}$ and $x(O) = 5 \times 10^{-5}$.

our inferred upper limit of 10^{-5}. Also, these models often do not allow for grain surface formation of H_2O. Our computed variation of the H_3O^+ and HCO^+ abundances with density depends, of course, on the assumed behavior of the CO, O, O_2, and H_2O abundances with density, which we take to be constant. If, e.g., CO and O were significantly depleted onto grains at $n > 10^6$ cm^{-3} (cf. Mezger et al. 1992), the H_3^+ abundance would be greatly enhanced (cf. eq. [3]). However, most sources studied here, in particular our primary source W3, are probably too warm for significant CO depletion. Another possible effect is that most of the atomic oxygen may be driven into O_2 at the higher densities, in which case the H_3O^+ abundance would be lowered somewhat but not that of HCO^+.

Finally, a limitation of the models is the fact that no recombination with dust grains has been taken into account. In particular, the presence of a large amount of very small grains or PAHs can significantly affect the abundances of the molecular ions through charge transfer and mutual neutralization. Lepp & Dalgarno (1988) demonstrate that for PAH abundances larger than 10^{-7} (corresponding to about 1% of the cosmic carbon abundance) these reactions are more effective than dissociative recombination for removal of ions such as H_3O^+. Because their rate coefficients are typically an order of magnitude smaller than for dissociative recombination, the abundances of the ions are greatly enhanced. In fact, for $x(PAH) \approx 10^{-6}$–10^{-7}, the computed steady-state abundances $x(H_3O^+) \approx 5 \times 10^{-8}$–$10^{-7}$ are so much larger than the observed values that such large PAH abundances can probably be excluded (Lepp & Dalgarno 1988).

5. COMPARATIVE DISCUSSION OF SOURCES

In this section we compare the various regions in which the H_3O^+ lines have been detected and comment on the differences in line strengths between the sources and in particular within the one region W3. It should be kept in mind, however, that the dynamic range of the observations is not large, at most a factor of a few, so that it is difficult to disentangle the various effects.

5.1. *The W3 Region*

The H_3O^+ observations presented in § 2.1 indicate that the ion is clearly detected at the W3 IRS 5 position, possibly at W3(OH), but not at the IRS 4 position. Is the absence of emission at IRS 4 due to different physical conditions, or are there real abundance variations across the cloud? Continuum (Richardson et al. 1989) and $C^{18}O$ observations (Keene et al. 1992; Wilson et al. 1991) indicate that the total column densities are similar at the three positions, $N(H_2) \approx 2 \times 10^{23}$ cm^{-2}. Moreover, the diagnostic observations discussed in § 3.5 indicate that the density at the positions is high enough to excite the 396 and 364 GHz lines, $n(H_2) > 5 \times 10^5$ cm^{-3}. Possible temperature differences are more difficult to establish. Analysis of the relative strength of various H_2CO lines indicates gas temperatures around 100–150 K toward IRS 5 and W3(OH), but somewhat lower temperatures, $T \approx 50$ K, toward IRS 4 (Helmich et al. 1992). Thus, a combination of small differences in density, column density and in particular temperature could explain the observed variations in H_3O^+ line strengths across W3, especially the absence of emission at the IRS 4 position. On the other hand, real H_3O^+ abundance variations of factors of 2–4 are a serious possibility.

Chemical differences between the IRS 5, IRS 4, and W3(OH) positions appear to occur for other species such as SO_2 and HCN (Wright, Dickel, & Ho 1984; Dickel et al. 1980, 1990), and CH_3OH (see below). Of most interest for the current discussion is the variation across the cloud of the abundances of other ions such as HCO^+, which is suggested by the HCO^+ and $H^{13}CO^+$ 1–0 observations of Hayashi et al. (1989) and Downes et al. (1982). In the simple chemical models discussed in § 4, such variations could occur if the gas phase water abundance were changing across the cloud. From the limit on the $H_2{}^{18}O$ 203 GHz line measured by Jacq et al. (1990) toward W3(OH), the limit on the H_2O column density is a few times 10^{17} cm^{-2} within a 30″ beam, corresponding to a water abundance of about 10^{-6}. HDO has been detected toward W3(OH), but the uncertainty in the fractionation prevents this from providing a stringent limit. Direct observations of the H_2O 183

GHz line were presented by Cernicharo et al. (1990), who saw a broad, presumably thermal component toward both IRS 5 and the W3(H_2O) position, which is located only 7″ away from W3(OH). For the physical conditions derived above, the inferred H_2O abundance is about (1–5) $\times$ 10^{-6} toward the two positions, averaged over a 14″ beam. Unfortunately, the analysis of the H_2O column densities is not accurate enough to determine differences of factors of a few between the two positions. The $H_2{}^{18}O$ ground state line at 548 GHz was searched toward IRS 4 with a beam large enough to encompass most of the W3 core (Wannier et al. 1991). The line was not detected, but their limit $H_2O/CO < 0.1$ or $x(H_2O) < 10^{-5}$ is not more stringent than those derived from the lower frequency lines. If the gas-phase H_2O abundance were 5×10^{-6} toward IRS 5, it would be larger than predicted from the observed H_3O^+ abundance on the basis of the simple chemistry outlined in § 4. As discussed in § 4.1, this would indicate that at least some of the observed H_2O does not result from gas-phase ion-molecule chemistry, but stems from formation on the grain surfaces followed by release back into the gas phase at high temperatures. At the IRS 4 position, however, the temperature may be too low for evaporation of H_2O, resulting in a lower gas-phase abundance of H_2O and consequently H_3O^+.

Alternative explanations for a varying H_3O^+ abundance and H_3O^+/HCO^+ ratio across W3 include a larger density toward IRS 5, which favors H_3O^+ relative to HCO^+ (cf. Fig. 14); variations in the atomic oxygen abundance, which is essentially unknown; and variations in the cosmic ray ionization rate. More detailed studies of the ion abundances in these clouds are warranted.

Another chemical difference between the three positions in W3 is formed by the CH_3OH abundance. As Figures 11 and 12 show, the CH_3OH 5_0–4_1 E and 8_1–7_2 E lines are much stronger toward W3(OH) and IRS 4 than toward IRS 5. A similar anticorrelation between H_3O^+ and CH_3OH is found for Orion. Based on the discussion above, this is unlikely to be an excitation effect. Current chemical models favor CH_3OH formation on the surfaces of the grains under the same hydrogen-rich conditions which form H_2O (Tielens & Allamandola 1987; Millar et al. 1991a). Since solid CH_3OH probably evaporates at a lower temperature than solid H_2O, a large gas phase CH_3OH abundance would have been expected toward IRS 5 as well, provided that no significant variations in the chemistry have occurred in the time span of less than 3×10^5 yr since evaporation. This is contrary to the observations. Perhaps the conditions toward IRS 5 favored formation of other molecules such as H_2CO, or maybe the CH_3OH lies more deeply embedded in the icy matrix and has not yet been released back into the gas phase. Evidence for different types of interstellar ices along a single line of sight has recently been presented by Tielens et al. (1991).

5.2. *Orion*

The probable detection of H_3O^+ toward Orion/KL reported by Wootten et al. (1991) has been strenghened by the current observations of the 396 GHz line, even though blends with other lines cannot be excluded. From our mapping, we find that the broad H_3O^+ line is not associated with the compact ridge as traced by CH_3OH, but centers on the hot core/plateau region. The relatively large H_2O abundance of 5×10^{-6}–10^{-5} in the hot core/plateau compared with, e.g., the extended ridge (Jacq et al. 1990; Wannier et al. 1991; Knacke & Larson 1991) certainly favors the production of H_3O^+ in that area, and the high densities ($n > 10^6$ cm^{-3}) clearly do not preclude observations of this ion, consistent with the weak density dependence shown in Figure 14.

H_3O^+ was not detected toward Orion FIR 4 and NGC 2024 FIR 5. On the basis of 1.3 mm continuum and $C^{18}O$ 2–1 observations, these regions are thought to have total column densities at least as large as those toward the W3 sources (Mezger et al. 1988, 1990; Keene et al. 1992). The absence of molecular lines in general in NGC 2024 FIR 5 is striking (cf. Mezger et al. 1992). Similarly, Groesbeck, Blake, & Phillips (1992) found the Orion FIR 4 region to be much less rich in molecules than Orion/KL. It is possible that these objects, like W3 IRS 4, are at an evolutionary state in which many species, including water and oxygen, are still depleted onto the grains, thus greatly inhibiting the gas-phase chemistry. The temperatures and densities at these positions certainly appear high enough to excite the H_3O^+ lines.

5.3. *Sgr B2*

The H_3O^+ found toward Sgr B2 is apparently in a different physical environment from that seen toward the other sources, as witnessed by the different [364/396] line ratio. Unless the 364 GHz line is a blend with another species, the observed ratio can only be explained if the H_3O^+ is in a rather low-density gas, $n \approx 10^4$–10^5 cm^{-3}, and if radiative excitation plays a role. Previous observations of other species indicate the presence of warm, very dense gas throughout Sgr B2, as well as an extended more diffuse component. Lis & Goldsmith (1991) derive $n \approx 10^5$ cm^{-3} and $T = 20$–40 K for this extended component from a HC_3N excitation analysis. Far-infrared continuum observations by Goldsmith et al. (1992) show that the extended dust emission has a 50/100 μm color temperature of 40 K. Such dust temperatures (or only slightly larger) would be sufficient to enhance the H_3O^+ 364 GHz line significantly over the 396 GHz line at low densities (cf. Fig. 13*c*). Indeed, evidence for radiative excitation of other molecules such as HNCO and HC_3N has been found in Sgr B2, especially at the 2′ N position, where the temperature of the radiation field may be significantly higher (Lis & Goldsmith 1991). Gas-phase H_2O is certainly present in substantial amounts toward Sgr B2 (Jacq et al. 1990), but its abundance toward the "M" and "OH" positions is more uncertain. The apparently low abundance of H_3O^+ in the high-density component at the "OH" position (as evidenced by the weakness of the 396 GHz line) suggests a low H_2O abundance there. The total H_2 column densities at our observed "OH" and 2′ N positions have been inferred from 1.3 mm continuum measurements and are 1×10^{24} and 4×10^{23} cm^{-2}, respectively (Lis, Carlstrom & Keene 1991).

5.4. *Other Sources*

Only a single position was observed for the other two regions, G34.3+0.15 and W51, toward which H_3O^+ has most likely been detected. G34.3+0.15 is a rich source of molecular line emission, including water (cf. Jacq et al. 1987; Strong-Jones, Heaton, & Little 1991). Similar parameters are thought to apply to W51 M, and are high enough to excite the H_3O^+ lines. The H_2 column density toward the two positions is at least as large as toward W3. Moreover, HDO and $H_2{}^{18}O$ lines have been detected toward both positions, and the inferred H_2O column densities are very similar. Thus, the detection of H_3O^+ in these regions at the observed level is not surprising, and it is plausible that in all these "hot core" regions with H_2O abundances of a few times 10^{-6}–10^{-5}, the H_2O with

H_3^+ formation route dominates. If the column density toward W51 M is indeed as high as (5–8) $\times 10^{23}$ cm^{-2}, its H_3O^+ abundance is significantly smaller than toward W3 IRS 5.

The absence of any detectable H_3O^+ emission toward the ρ Oph A sources may simply result from the fact that these clouds are somewhat colder and have smaller total column densities. However, for the IRAS 16293−2422 protostellar region, a gas temperature $T \approx 80$ K and density $n \approx 5 \times 10^6$ cm^{-3} have been found (Blake et al. 1992), so that the conditions for excitation of H_3O^+ should be favorable. Moreover, the total column density averaged over a 20″ beam is similar to that of W3 (Mundy, Wootten, & Wilking 1990). The resulting upper limit on the H_3O^+ abundance for these conditions of only 5×10^{-11} is the most significant limit we have obtained, and is substantially lower than predicted by the simple chemical models. In analogy with the W3 IRS 4 case, a possible explanation would be that the temperature is still just below the threshold at which H_2O is released back into the gas phase and that in addition the gas-phase atomic oxygen abundance is fairly low.

6. CONCLUSIONS

We have searched for three different submillimeter transitions of H_3O^+, and have definitely detected the ion toward W3 IRS 5 and G34.3+0.15, and very likely toward Orion/KL, Sgr B2, W3(OH) and W51 M. The observed [396/364] antenna temperature ratios of about 2 in most sources are well explained by excitation models with high densities ($n > 10^6$ cm^{-3}) and high temperatures ($T \gtrsim 50$ K). The major exception is the case of Sgr B2, for which a much lower [396/364] ratio is found. This probably indicates that in Sgr B2, the H_3O^+ is located in lower density ($n \approx 10^5$ cm^{-3}) gas in which radiative pumping by far-infrared dust emission plays a role. The 307 GHz line is always very weak and is only observed in very high-density regions where $n > 10^7$ cm^{-3}.

The derived H_3O^+ abundances of typically 10^{-10}–10^{-9} are consistent with, or slightly below the predictions of simple chemical models in which the ion is formed by reactions of H_3^+ with O and H_2O. Conversely, the observed H_3O^+ abundances have been used here to provide an order-of-magnitude prediction of the amounts of O_2 and H_2O in the clouds, if the formation of these species results primarily from dissociative recombination of the ion. The derived O_2 abundances of 10^{-6}–10^{-5} are comparable to the best measured upper limits of about 10^{-5} obtained from $^{16}O^{18}O$ searches, and are lower than the O_2 abundances found in most standard gas-phase models. The inferred H_2O abundances in regions where the ion has been detected are about 10^{-7}–10^{-6}, which are somewhat lower than the gas-phase H_2O abundances derived from other observations. In these cases, an additional source of H_2O, presumably through surface reactions on grains with subsequent evaporation back into the gas phase, may be required. The absence of H_3O^+ emission in other sources (or even at different positions within the same source) may be caused by a variety of chemical and physical effects. The temperature in the cloud clearly plays a crucial role, since it is important both in the excitation of the H_3O^+ lines and in the release of water mantles from the grains. Neither O_2 nor H_2O appears to contain a significant fraction of the available oxygen, so the details of the oxygen chemistry in interstellar clouds remain uncertain, and it can be presumed that much remains bound in some way to the grains.

The definite identification of H_3O^+ in a number of sources represents a significant step forward, verifying the primary processes in the ion-molecule reaction scheme, and providing a prediction of gas-phase O_2 and H_2O.

The authors are much indebted to the CSO staff for their help and support, in particular to Antony Schinckel, Larry Strom, and Thomas Büttgenbach for assistance with part of the observations. They are grateful to J. H. Black and G. A. Blake for useful discussions regarding the chemistry, to A. R. Offer for performing the collisional calculations, and to D. Lis for helpful comments on Sgr B2. This work was supported by NSF contract AST 90-15755 to the California Institute for Technology, and by a PIONIER grant from the Netherlands Organization for Scientific Research (NWO).

APPENDIX

Here we briefly discuss the line identification for the other features in the spectra. Table 3 gives a list of the more clearly defined features in the 396, 364, and 307 GHz bands, together with the image sidebands, for the Orion KL spectra, with identifications where possible. The identifications are made on the basis of the catalogs of Poynter & Pickett (1985) and Lovas (1984) and the recent papers by Anderson, Herbst, & De Lucia (1992) for $^{13}CH_3OH$ and CH_3OH. Wootten et al. (1991) also analyze the 364 GHz band, which is by far the most complex.

Methanol, in its ground and torsionally excited states and in its ^{13}C isotopic form, is well represented in the spectra. See also Sutton et al. (1985) and Blake et al. (1987) for a discussion of methanol in Orion. In part the number of identified methanol lines is due to the excellent laboratory and theoretical work which exists for this species, resulting in complete catalogs of lines, e.g., Anderson, Herbst, & De Lucia (1992). The process of searching for the chemically interesting species such as H_3O^+ is clearly very much aided by as much knowledge as possible on spectroscopically prolific species such as CH_3OH.

Such lines are seen in many of the sources. The lower lying methanol lines are quite common, but also the OCS/DCN and the U 396.358 line. This last is a strong feature and, although probably blended in the Orion spectrum, is seen alone in Orion FIR 4, W3 (OH), W51 and G34.3+0.15. However, it is not in Sgr B2.

The amazing proliferation of lines in the submillimeter band and the fact that a significant fraction are not in the current catalogs indicates the large amount of work still required in this field if chemically interesting, but weak lines are to be easily identified.

TABLE 3

IDENTIFICATION OF OTHER LINES

Frequency (GHz)	Assignment
396 and 398 GHz Bands	
396.162	None
396.272	H_3O^+ 3_0–2_0
396.358	None
396.517	$^{13}CH_3OH$ 2_1–1_0 (A)
398.946	CH_3OH 5_0–4_1 (E)
364 GHz and 362 GHz Bands	
361.836	None
361.852	CH_3OH 8_1–7_2 (E)
361.865	None
361.876	None
361.894	None
361.949	? NH_2CHO 17–16?
362.046	DCN 5–4 [blended with OCS and CH_3OH]
362.101	None
362.149	CH_3OH $v_t = 1$ 12_3–12_2 (E)
362.159	None
362.192	None
362.212	None
362.223	None
364.640	None
364.680	? HNO_3 17–16?
364.746	CH_3OH $v_t = 1$ 7_3–7_2 (E) blended with DCN
364.749	OCS 30–29 blended with DCN
364.797	H_3O^+ 3_2–2_2
364.836	None
364.898	CH_3OH $v_t = 1$ 6_3–6_2 (E)
364.987	CH_3OH $v_t = 1$ 5_3–5_2 (E)
365.031	CH_3OH $v_t = 1$ 4_3–4_2 (E)
365.047	CH_3OH $v_t = 1$ 3_3–2_2 (E) off the end of the spectrum shown, but present in other data
307 GHz and 304 GHz Bands	
304.210	CH_3OH 2_1–2_0 (A)
304.306	H_2CS 9_{19}–8_{18}
307.090 (or 304.495)	None
307.166	CH_3OH 4_1–4_0 (A)
307.192	H_3O^+ 1_1–2_1
307.209 (or 304.375)	? CH_3CCH 18_8–17_8 ?
307.311	$^{13}CH_3OH$ 4_1–4_0 (A)

REFERENCES

Anderson, T., Herbst, E., & De Lucia, F. C. 1992, ApJS, 82, 405
Bates, D. R. 1991, J. Phys. B, 24, 3267
Becklin, E. E., Matthews, K., Neugebauer, G., & Willner, S. P. 1978, ApJ, 220, 831
Bergman, P., Hjalmarson, Å., & Booth, R. 1992, A&A, submitted
Black, J. H., & Smith, P. L. 1984, ApJ, 277, 562
Black, J. H., van Dishoeck, E. F., Willner, S. P., & Woods, R. C. 1990, ApJ, 358, 459
Blake, G. A., Sutton, E. C., Masson, C. R., & Phillips, T. G. 1987, ApJ, 315, 621
Blake, G. A., et al. 1992, in preparation
Bogey, M., Demuynck, C., Denis, M., Destombes, J. L. 1985, A&A, 148, L11
Boreiko, R. T., & Betz, A. L. 1991, ApJ, 369, 382
Botschwina, P., Rosmus, P., & Reinsch, E. A. 1983, Chem. Phys. Lett., 102, 299
Brown, P. D., Charnley, S. B., & Millar, T. J. 1988, MNRAS, 231, 409
Cernicharo, J., Thum, C., Hein, H., John, D., Garcia, P., & Mattioco, F. 1990, A&A, 231, L15
Cheung, A. C., Rank, D. M., Townes, C. H., Thornton, D. D., & Welch, W. J. 1969, Nature, 221, 626
Combes, F., Casoli, F., Encrenaz, P., Gerin, M., & Laurent, C. 1991, A&A, 248, 607
Cummins, S. E., Linke, R. A., & Thaddeus, P. 1986, ApJS, 60, 819
Dalgarno, A., & Black, J. H. 1976, Rep. Progr. Phys., 39, 573
Dickel, H. R., Dickel, J. R., Wilson, W. J., & Werner, M. W. 1980, ApJ, 237, 711
Dickel, H. R., Kameya, O., Deguchi, S., Hirano, N., & Sircar, K. 1990, BAAS, 22, 797
Downes, D., Genzel, R., Hjalmarson, Å., Nyman, L. Å., & Rönnäng, B. 1982, ApJ, 252, L29
Ellison, B. N., Schaffer, P. L., Schaal, W., Vail, D., & Miller, R. E. 1989, Int. J. Infrared Millimeter Waves, 10, 937
Georgelin, Y. M., & Georgelin, Y. P. 1976, A&A, 49, 57
Goldsmith, P. F., Lis, D. C., Lester, D. F., & Harvey, P. M. 1992, ApJ, 389, 338
Goldsmith, P. F., Snell, R. L., Erickson, N. R., Dickman, R. L., Schloerb, F. P., & Irvine, W. M. 1985, ApJ, 289, 613
Gordon, M. A. 1987, ApJ, 316, 258
Groesbeck, T., Blake, G. A., & Phillips, T. G. 1992, in preparation
Hayashi, M., Kobayashi, H., & Hasegawa, T. 1989, ApJ, 340, 298
Heaton, B. D., Little, L. T., & Bishop, I. S. 1989, A&A, 213, 148
Helmich, F. P., Jansen, D. J., van Dishoeck, E. F., & de Graauw, T. 1992, in preparation
Henkel, C., Wilson, T. L., & Mauersberger, R. 1987, A&A, 182, 137
Herbst, E., Green, S., Thaddeus, P., & Klemperer, W. 1977, ApJ, 215, 503
Herbst, E., & Klemperer, W. 1973, ApJ, 185, 505
Herbst, E., & Leung, C. M. 1989, ApJS, 69, 271
Herd, C. R., Adams, N. G., & Smith, D. 1990, ApJ, 349, 388
Hollis, J. M., Churchwell, E. B., Herbst, E., & De Lucia, F. C. 1986, Nature, 322, 524
Jacq, T., Jewell, P. R., Henkel, C., Walmsley, C. M., & Baudry, A. 1988, A&A, 199, L5
Jacq, T., Walmsley, C. M., Henkel, C., Baudry, A., Mauersberger, R., & Jewell, P. R. 1990, A&A, 228, 447

Jaffe, D. T., Hildebrand, R. H., Keene, J., & Whitcomb, S. E. 1983, ApJ, 273, L89
Keene, J. B., van Dishoeck, E. F., Black, J. H., & Phillips, T. G. 1992, in preparation
Knacke, R. F., & Larson, H. P. 1991, ApJ, 367, 162
Krolik, J. H., & Kallman, T. R. 1983, ApJ, 267, 610
Krügel, E., et al. 1989, A&A, 211, 419
Langer, W. D., & Graedel, T. E. 1989, ApJS, 69, 241
Lepp, S., & Dalgarno, A. 1988, ApJ, 324, 553
Lepp, S., Dalgarno, A., & Sternberg, A. 1987, ApJ, 321, 383
Lis, D. C., Carlstrom, J. E., & Keene, J. 1991, ApJ, 380, 429
Lis, D. C., & Goldsmith, P. F. 1989, ApJ, 337, 704
———. 1991, ApJ, 369, 157
Liszt, H. A., & Vanden Bout, P. A. 1985, ApJ, 291, 178
Liu, D. J., & Oka, T. 1985, Phys. Rev. Lett., 54, 1787
Loren, R. B., Wootten, A., & Wilking, B. A. 1990, ApJ, 365, 269
Lovas, F. J. 1984, private communication
Mamon, G. A., Glassgold, A. E., & Omont, A. 1987, ApJ, 323, 306
Mangum, J. G., Wootten, A., Loren, R. B., & Wadiak, E. J. 1990, ApJ, 348, 542
Menten, K. M., Melnick, G. J., & Phillips, T. G. 1990a, ApJ, 350, L41
Menten, K. M., Melnick, G. J., Phillips, T. G., & Neufeld, D. A. 1990b, ApJ, 363, L27
Mezger, P. G., Chini, R., Kreysa, E., Wink, J. E., & Salter, C. J. 1988, A&A, 191, 44
Mezger, P. G., Sievers, A. W., Haslam, C. G. T., Kreysa, E., Lemke, R., Mauersberger, R., & Wilson, T. L. 1992, A&A, 256, 631
Mezger, P. G., Wink, J. E., & Zylka, R. 1990, A&A, 228, 95
Millar, T. J., Herbst, E., & Charnley, S. B. 1991a, ApJ, 369, 147
Millar, T. J., Rawlings, J. M. C., Bennett, A., Brown, P. D., & Charnely, S. B. 1991b, A&AS, 87, 585
Minh, Y. C., Irvine, W. M., & Ziurys, L. M. 1988, ApJ, 334, 175
Monteiro, T. S. 1984, MNRAS, 210, 1
———. 1985, MNRAS, 214, 419
Mundy, L. G., Wootten, H. A., & Wilking, B. A. 1990, ApJ, 352, 159
Offer, A. R., & Flower, D. R. 1989, J. Phys. B, 22, L439
Offer, A. R., & van Dishoeck, E. F. 1992, MNRAS, in press
Offer, A. R., & van Hemert, M. C. 1992, Chem. Phys., in press
Phillips, T. G., Knapp, G. R., Huggins, P. J., Werner, M. W., Wannier, P. G., Neugebauer, G., & Ennis, D. 1981, ApJ, 245, 512
Phillips, T. G., Kwan, J., & Huggins, P. J. 1980, in IAU Symp. 87, Interstellar Molecules, ed. B. H. Andrew (Dordrecht: Reidel), 21
Phillips, T. G., Scoville, N. Z., Kwan, J., Huggins, P. J., & Wannier, P. G. 1978, ApJ, 222, L59
Plambeck, R. L., & Wright, M. C. H. 1987, ApJ, 317, L101
Plummer, G. M., Herbst, E., & De Lucia, F. C. 1985, J. Chem. Phys., 83, 1428
Poynter, R. L., & Pickett, H. M. 1985, Appl. Opt., 24, 2235
Richardson, K. J., Sandell, G., White, G. J., Duncan, W. D., & Krisciunas, K. 1989, A&A, 221, 95
Schulz, A., Güsten, R., Serabyn, E., & Walmsley, C. M. 1991, A&A, 246, L55
Schwartz, P. R., Snell, R. L., & Schloerb, F. P. 1989, ApJ, 336, 519
Strong-Jones, F. S., Heaton, B. D., & Little, L. T. 1991, A&A, 251, 263
Sutton, E. C., Blake, G. A., Masson, C. R., & Phillips, T. G. 1985, ApJS, 58, 341
Sutton, E. C., Jaminet, P. A., Danchi, W. C., & Blake, G. A. 1991, ApJS, 77, 255
Thronson, H. A., Jr., & Harper, D. A. 1979, ApJ, 230, 133
Tielens, A. G. G. M., & Allamandola, L. J. 1987, in Interstellar Processes, ed. D. J. Hollenbach & H. A. Thronson (Dordrecht: Reidel), 397
Tielens, A. G. G. M., Tokunaga, A. T., Geballe, T. R., & Baas, F. 1991, ApJ, 381, 181
Townes, C. H., & Schawlow, A. L. 1955, Microwave Spectroscopy (NY: Dover)
Turner, B. E. 1991, ApJS, 76, 617
Turner, B. E., Zuckerman, B., Fourikis, N., Morris, M., & Palmer, P. 1975, ApJ, 198, L125
Verhoeve, P., ter Meulen, J. J., Meerts, W. L., & Dymanus, A. 1988, Chem. Phys. Lett., 143, 501
Verhoeve, P., Versluis, M., ter Meulen, J. J., Meets, W. L., & Dymanus, A. 1989, Chem. Phys. Lett., 161, 195
Wannier, P. G., et al. 1991, ApJ, 377, 171
Waters, J. W., et al. 1980, ApJ, 235, 57
Werner, M. W., et al. 1980, ApJ, 242, 601
Wilson, T. L., Johnston, K. J., Henkel, C., & Menten, K. M. 1989, A&A, 214, 321
Wilson, T. L., Johnston, K. J., & Mauersberger, R. 1991, A&A, 251, 220
Wootten, A., Boulanger, F., Bogey, M., Combes, F., Encrenaz, P. J., Gerin, M., & Ziurys, L. 1986, A&A, 166, L15
Wootten, A., Boulanger, F., Zhou, S., Combes, F., Encrenaz, P., Gerin, M., & Bogey, M. 1990, in Submillimetre Astronomy, ed. G. D. Watt & A. S. Webster (Dordrecht: Kluwer), 107
Wootten, A., & Loren, R. B. 1987, in Molecular Clouds in the Milky Way and External Galaxies, ed. R. L. Dickman, R. L. Snell, & J. S. Young (Münich: Springer), 178
Wootten, A., Mangum, J. G., Turner, B., Bogey, M., Boulanger, F., Combes, F., Encrenaz, P. J., & Gerin, M. 1991, ApJ, 380, L79
Wright, M. C. H., Dickel, H. R., & Ho, P. T. P. 1984, ApJ, 281, L71
Wynn-Williams, C. G., Becklin, E. E., & Neugebauer, G. 1972, MNRAS, 160, 1
Zmuidzinas, J., Betz, A., & Goldhaber, D. 1986, ApJ, 307, L79